MIGMATITES OF THE MUSKOKA DOMAIN, GRENVILLE PROVINCE, ONTARIO

Tracy A. Gray

Submitted in Partial Fulfillment of the Requirements
for the Degree of Bachelor of Science, Honours
Department of Earth Sciences
Dalhousie University, Halifax, Nova Scotia
March, 1998

Distribution License

DalSpace requires agreement to this non-exclusive distribution license before your item can appear on DalSpace.

NON-EXCLUSIVE DISTRIBUTION LICENSE

You (the author(s) or copyright owner) grant to Dalhousie University the non-exclusive right to reproduce and distribute your submission worldwide in any medium.

You agree that Dalhousie University may, without changing the content, reformat the submission for the purpose of preservation.

You also agree that Dalhousie University may keep more than one copy of this submission for purposes of security, back-up and preservation.

You agree that the submission is your original work, and that you have the right to grant the rights contained in this license. You also agree that your submission does not, to the best of your knowledge, infringe upon anyone's copyright.

If the submission contains material for which you do not hold copyright, you agree that you have obtained the unrestricted permission of the copyright owner to grant Dalhousie University the rights required by this license, and that such third-party owned material is clearly identified and acknowledged within the text or content of the submission.

If the submission is based upon work that has been sponsored or supported by an agency or organization other than Dalhousie University, you assert that you have fulfilled any right of review or other obligations required by such contract or agreement.

Dalhousie University will clearly identify your name(s) as the author(s) or owner(s) of the submission, and will not make any alteration to the content of the files that you have submitted.

If you have questions regarding this license please contact the repository manager at dalspace@dal.ca.

Grant the distribution license by signing and dating below.

_____ _____

Name of signatory Date

Dalhousie University

Department of Earth Sciences
Halifax, Nova Scotia
Canada B3H 3J5
(902) 494-2358
FAX (902) 494-6889

DATE MARCH 16, 1998

AUTHOR TRACY A. GRAY

TITLE MIGMATITES OF THE MUSKOKA DOMAIN, GRENVILLE PROVINCE, ONTARIO

Degree B.Sc. Convocation MAY Year 1998

Permission is herewith granted to Dalhousie University to circulate and to have copied for non-commercial purposes, at its discretion, the above title upon the request of individuals or institutions.

Abstract

The Muskoka Domain, Central Gneiss Belt, Grenville Province, Ontario, is characterized by widespread highly migmatitic orthogneisses. The purpose of this study is to describe a variety of migmatites and associated rocks from a small section representative of the Muskoka Domain, using detailed petrographic descriptions and microprobe analyses. The amount of leucosome in outcrop ranges from 10 to 35%. Thirty-eight samples were classified into 4 types based on the amount and shape of leucosome, and the presence of mafic porphyroblasts in the leucosome. Non-migmatitic fine-grained mafic rocks from discrete layers in the migmatites comprise Type 1. Type 2 migmatites are characterized by thin ($\leq$ 1 cm wide), stringy leucosome patches, parallel to or cross-cutting the foliation. Type 3 migmatites are stromatic, with variable leucosome width. Type 4 migmatites are characterized by hornblende and/or biotite porphyroblasts in the coarse-grained leucosomes, typically parallel to and cross-cutting the foliation. Deformation in Type 4 migmatites is illustrated by large quartz ribbons (~ 2 cm), myrmekite, mosaic texture in quartz and felspars, cross-hatch twinned microcline, and finer-grained recrystallized matrix in leucosomes. All leucosomes are enriched in potassium feldspar relative to mesosome and/or melanosome; Type 4 leucosomes are also quartz-rich. The typical mineral assemblage of a mesosome is hb+pl+bt+kf+opq+qz. Microprobe analyses for each group of minerals are fairly uniform. Some samples have slightly more calcic plagioclase and more potassic alkali feldspars in the mesosome, and biotite and hornblende are more magnesian in some samples. These data are consistent with the formation of leucosome by partial melting. However, general similarity of feldspar compositions between leucosome and host, and abundance of leucosome in outcrop, suggest extensive equilibration of melt with host and limited migration.

Key Words: migmatite, petrogenesis, melt migration, anatexis, stromatic, orthogneiss, Muskoka Domian, Central Gneiss Belt

TABLE OF CONTENTS

TABLE OF FIGURES

TABLE OF TABLES

TABLE OF ABBREVIATIONS

alter	alteration
ap	apatite
bdaries	boundaries
bt	biotite
cal	calcite
fdsprs	feldspars
hb	hornblende
inequi.	Inequigranular
leuc	leucosome
kf	potassium feldspar
meso	mesosome
melan	melanosome
min.s	minerals
musc	muscovite
opq	opaque minerals
opx	orthopyroxene
p'blasts	porphyroblasts
pl	plagioclase feldspar
PPL	plane polarized light
ti	titanite
qz	quartz
XN	crossed nickels
zr	zircon

Acknowledgements

This thesis would not have been possible without the support and guidance of my advisor, Dr. R.A. Jamieson. Hilke Timmermann has also provided tremendous support by preparing me for the field, and for multiple helpful discussions thereafter. My field assistants deserve mention for their tremendous patience—thank you Brandon and Kayla. I would also like to thank Gordon Brown for the thin section preparation, Bob Mackay for his guidance on the microprobe, and Cal Jackson for assistance with the staining procedures at DalTech. Finally, I would like to thank all of my classmates for helping me through the "thesis experience".

CHAPTER 1 – INTRODUCTION

1.0 Introduction

Migma is Greek for mixture. Loosely defined, a migmatite is a mixed rock. Ashworth (1985) defines migmatite as "a rock found in medium-grade to high-grade metamorphic areas, that is pervasively inhomogeneous on a macroscopic scale, one part being pale-coloured...". This study will focus on the description of different migmatite samples and associated rocks in a small area of the Muskoka Domain, Grenville Province, Ontario. The Muskoka Domain consists predominantly of migmatitic gneisses, with shallow foliations and moderate dips (Culshaw et al., 1983).

The Muskoka Domain is very interesting from a tectonic point of view; it represents the immediate footwall of the overlying Central Metasedimentary Belt boundary thrust zone. The migmatites are concentrated in a region between allochthonous rock above, and underlying rocks of the Laurentian craton. The migmatites may have formed as a result of deep burial, or partial subduction of Laurentia beneath the Central Metasedimentary Belt (Culshaw et al., 1997). A detailed study of the migmatites of the Muskoka Domain has not previously been carried out.

Mehnert (1968) completed the first comprehensive book concerning migmatites and granite petrogenesis. Due mainly to changes in terminology, his work is only marginally referred to in this thesis, but the significance of his work should not be overlooked. Yardley (1978) effectively discussed possible mechanisms for the development of migmatites, which forms the basis of this study – how did these migmatites form? Ashworth (1985) compiled a book that is referred to commonly in this thesis. His book constitutes petrological review articles of the current migmatite researchers of the time. Recent work compiled by Brown et

articles of the current migmatite researchers of the time. Recent work compiled by Brown et al. (1995) concern the consequences and mechanisms of melt segregation. Laboratory experiments focus on melting and segregation processes, and the ascent and emplacement of magma. The effects of deformation on partially molten rock is also being examined (e.g. Rushmer, 1995; Rutter and Neuman, 1995).

1.1 Objectives

The purpose of this thesis is to provide systematic descriptions of 38 samples, representing a range of migmatite types and associated rocks within the Muskoka Domain. It will be achieved through detailed petrographic descriptions and microprobe analysis. An attempt will also be made to determine the origin of the migmatites according to Yardley's (1978) classification.

1.2 Approach and Methods

Samples were taken from three adjacent outcrops on highway 117 west of Baysville, Ontario, and from highway 11 south of Bracebridge (Fig. 1.1). A wide variety of migmatites is present within this area. The samples were subsequently grouped according to the amount and shape of leucosome, and the presence of mafic porphyroblasts. Normal and polished thin sections were made from representative samples of each group. Detailed petrographic descriptions were preformed, and microprobe analysis was used to confirm mineral identification and to note variations in composition.

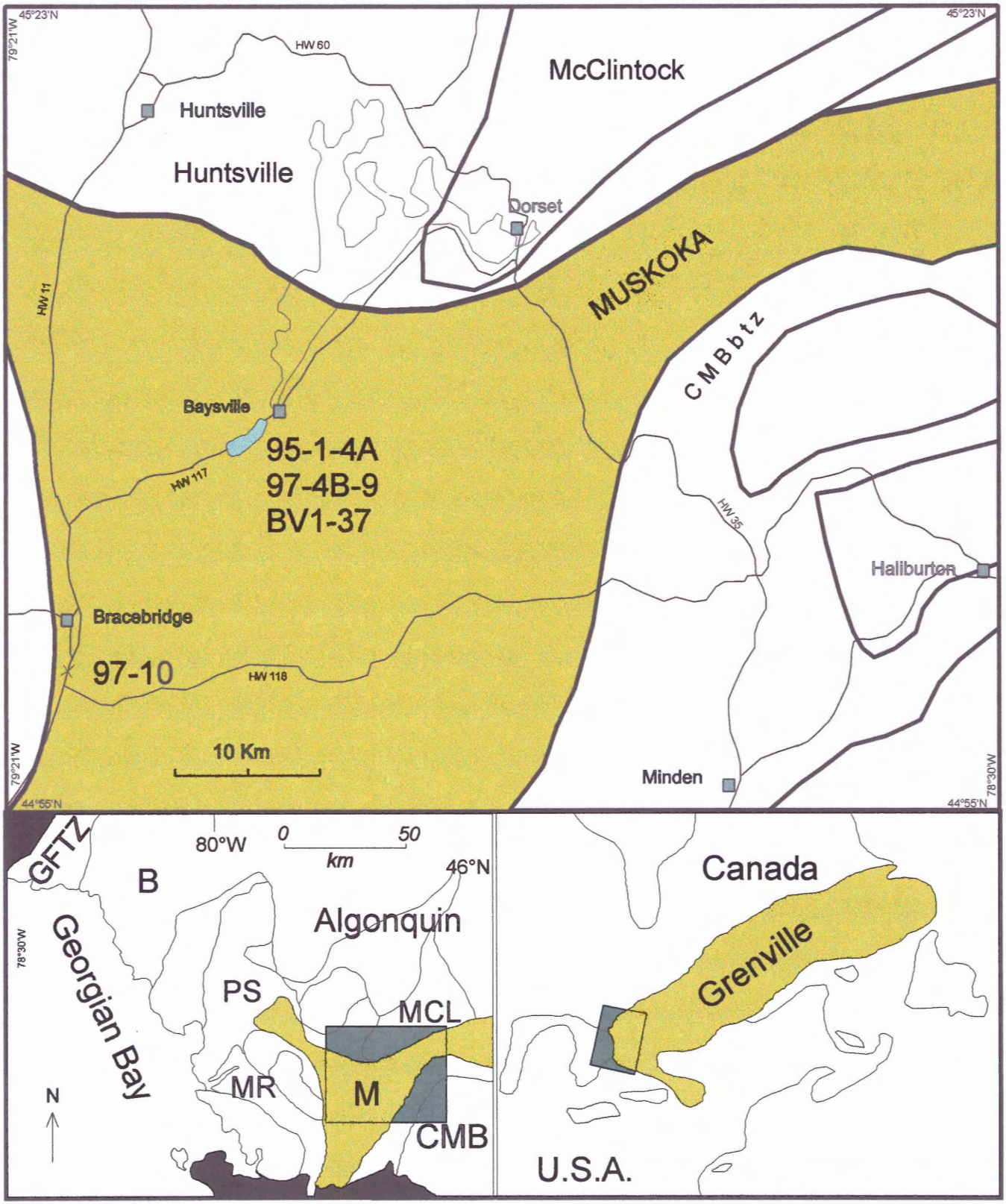

Figure 1.1. Simplified geological map of the study area in the Central Gneiss Belt of Ontario (modified after Davidson et al. 1984; Culshaw et al. 1990; Timmermann et al. 1997). It shows the lithotectonic domains of the Central Gneiss Belt and sample locations in the Muskoka Domain. GFTZ=Grenville Front Tectonic Zone; CMB=Central Metasedimentary Belt; CMBbtz=Central Metasedimentary Belt boundary thrust zone; M=Muskoka Domain.

1.3 Origin and Classification of Migmatites

The terminology that Ashworth (1985) uses will be followed in this thesis. Two distinct bodies within migmatites are the *leucosome* and the *melanosome* (Fig. 1.2). The leucosome is the pale-coloured, quartzofeldspathic or feldspathic lithology of the migmatite, whereas the melanosome, which is complementary to the leucosome, is rich in mafic minerals, and typically forms a selvage on leucosome. The *neosome* consists of leucosome and melanosome. The *mesosome* is the body of the migmatite complex that is not neosome, and is typically intermediate in colour between leucosome and melanosome. These definitions and others relevant to this thesis are presented in Table 1.1.

Migmatites may form by igneous processes (in the presence of silicate melt), or by hydrothermal processes (Yardley, 1978). A summary of possible migmatization mechanisms is presented in Table 1.2. Each mechanism is considered separately, however in any given case, migmatization may have been caused by a combination.

Experimental studies are not very useful when considering *igneous injection* as a method of migmatization. This is directly the result of the wide variety of igneous melts that may be injected into a similarly wide variety of country rocks. Typical rock type formed by igneous injection is intrusion breccia. Documented examples of this type of migmatization can be seen on the margins of the Thorr and Fanad plutons in Donegal (Pitcher and Berger, 1972).

Experimental studies of partial melting have been done for plagioclase-bearing systems. The albite component of plagioclase fractionates so that, following crystallization, plagioclase in granitic leucosomes should be more sodic (i.e. 10-40% Ab) than in the melanosome. (This is considered in more detail in Chapter 5.) This differentiation has been

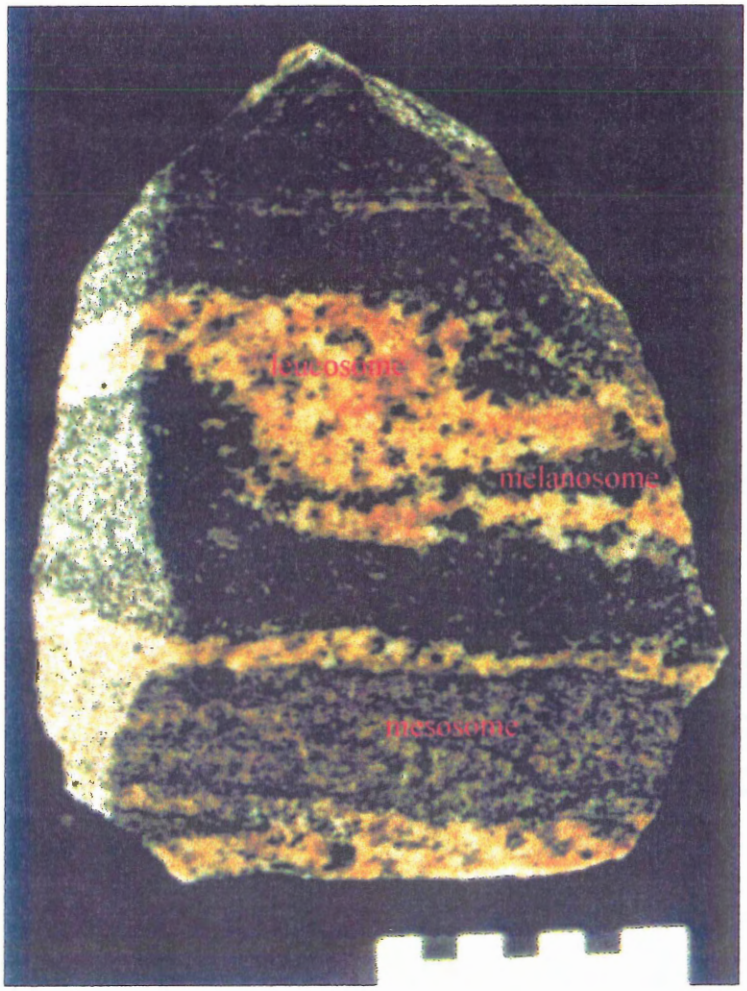

Figure 1.2. Sample 97-7 illustrating the three different components of migmatites:
(1) leucosome: pale-coloured quartzofeldspathic lithology;
(2) melanosome: mafic-rich component, typically forms a selvage on leucosome;
(3) mesosome: body of migmatite that is not leucosome or melanosome, typically intermediate in colour.

Table 1.1 – Definitions

Bodies within a migmatite	
Leucosome	pale-coloured quartzofeldspathic or feldspathic lithology
Melanosome	rich in mafic minerals, complementary to leucosome
Neosome	Leucosome and melanosome
Mesosome	body of migmatite that is not neosome, often intermediate in colour
Protolith	Hypothetical parent rock which developed into neosome
Restite	residual body, material left over, more mobile material has been extracted
Mobilizate	mobile material extracted from restite
Structural types of migmatite	
Stromatic	layered (usually rather irregularly)
Schlieren	streaks of non-leucosome in leucosome
Schollen	blocks or rafts of non-leucosome in leucosome
Terms related to melting	
Anatexis	partial melting in situ, with only small amount of melt segregation
Metatexis	Moderate amount of partial melting, leucosome subordinate to Remaining rock, no disruption of pre-migmatization structures
Diatexis	Extensive partial melting, leucosome volumetrically equal to or greater than remaining rock, disruption of pre-migmatization structures, often prominent mafic minerals in leucosome

Modified after Ashworth (1985).

observed in some migmatites, however, in many cases there is little difference between the plagioclase compositions of the leucosome and melanosome.

Table 1.2 - Possible Migmatization Mechanisms

	Open System	Closed System
Igneous process	igneous injection	anatexis
Hydrothermal process	external metasomatism	metamorphic segregation

After White (1966), Misch (1968), and Yardley (1978).

Metasomatism is a hydrothermal process involving the transport of material through intergranular fluid. Chemical potential gradients may cause the recrystallization of minerals in veins within the host rock. The gradient is controlled by the layer in which the vein develops and is termed *internal metasomatism* or *metamorphic segregation*. There is no change in the composition of the entire layer, including the vein. When the chemical potential gradient is controlled by an external source (e.g. an adjacent layer of different composition, or fluid from an external source), *external metasomatism* results. This causes a change in composition of the layer in which the vein develops. Both hydrothermal processes imply a fracture system resulting in a veined migmatite.

1.4 Organization

Chapter two describes the lithology of the study area, sample characteristics and their classification. Chapter three examines the petrography of chosen samples. Mineral chemistry

is examined in Chapter four. Interpretations are presented in Chapter five, and brief conclusions are in Chapter 6.

CHAPTER 2 — FIELD RELATIONS AND LITHOLOGY

2.1 Regional Geological Setting

The Grenville orogeny was caused by the accretion of the ca. 1100-1300 magmatic arcs and/or continental terranes of the Central Metasedimentary Belt (CMB) onto the pre-1400 Ma Laurentian craton, now called the Central Gneiss Belt (CGB) (Fig. 1.1). The contact between the CMB and CGB is a crustal-scale imbricate thrust zone referred to as the Central Metasedimentary Belt boundary thrust zone (CMBbtz). The Muskoka Domain lies structurally below the CMBbtz (within the CGB), and is considered to represent the immediate footwall. The exact time of emplacement is controversial, but was between 1190 Ma and 1080 Ma. It is generally assumed that collision initiated crustal thickening and metamorphism in the underlying footwall (of the CGB) (Timmermann et al., 1997). Timmerman et al. (1997) found ages of 1079—1064 Ma for high-grade metamorphism and anatexis within the Muskoka Domain from U-Pb zircon and titanite data.

The dominant rock type in the Muskoka Domain is grey to pink migmatitic orthogneiss (Timmerman et al., 1997). Metamorphic grade is generally at amphibolite facies in the Muskoka Domain; however relict clinopyroxene and orthopyroxene locally rimming amphibole (Fig. 2.1) suggest earlier granulite facies metamorphism. The amount of leucosome within migmatites may reach 35%. The leucosomes are typically less than 5 cm wide, but may be 50 cm wide. They may contain hornblende and biotite porphyroblasts up to 2 cm in size.

Figure 2.1. Relict pyroxene rim hornblende or biotite in coarse-grained leucosome. The coarser-grained leucosome cuts the foliation and two smaller leucosomes at the bottom.

2.2 Outcrop Characteristics

Three laterally adjacent outcrops (approximately 3km) on Highway 117 west of Baysville, Ontario were visited in July, 1997 (Fig. 1.1). These outcrops, which consist dominantly of migmatitic orthogneisses, contain a variety of lithologies and textures representative of the Muskoka Domain migmatites (Timmermann pers. com., 1997). The outcrop surfaces are at high angle to the lineation, therefore the cross-cutting features are well illustrated. The top of the outcrops (parallel to the lineation) exhibits the strongly deformed rocks.

The orthogneisses exhibit a dominant planar fabric striking roughly north, dipping shallowly to the east. This differs slightly from the general trend of the Muskoka Domain which strikes northeast, dipping southeast. Lineations consistently plunge to the southeast. Approximately 50% of the migmatites may be described as *stromatic*, due to their dominantly planar fabric (Fig. 2.2). They may also be wavy, or contain leucosomes with discontinuous blocks or rafts, called *schollen* (Fig. 2.3). Continuous mafic amphibolite or granulite layers occur up to tens of metres in length, as boudinaged lenses, or as discrete enclaves up to 2 m in length (Fig. 2.4).

The mesosome (i.e. host rock) constitutes the largest portion of the outcrops. They are dominantly granodioritic orthogneisses, with some more mafic varieties. Mesosome are typically interpreted as the rocks prior to migmatite formation (i.e. likely protoliths).

The darkest component in the migmatite system is the melanosome. It typically forms a finer-grained biotite- or hornblende-rich selvage on leucosome. The melanosome is the least abundant part of the migmatite complex.

The pale-coloured leucosomes range in colour from light grey to dark pink. They may occur parallel to, or discordant to the layering, or form diffuse patches (Fig. 2.5) in a wide

Figure 2.2. A) Typical stromatic migmatite with minor amounts of biotite and/or hornblende porphyroblasts in the leucosomes. Although they are stromatic, the leucosomes can also be wavy. Similarly, the width of one particular leucosome can change considerably. There is a significant range in leucosome width. B) This photograph illustrates the lateral continuity of banding in the stromatic migmatites that is prevalent in the study area. Brandon's hand points to a mafic (amphibolite?) layer parallel to the layering, and there are many others in the photo. In the southwest corner there is an abrupt transition to schollen migmatites.

Figure 2.3. A) Layering still visible in block of mesosome (?) in leucosome. The leucosome is filling the boudin necks. The layering is also showing a minor pinch and swell structure. Immediately to the east of the boudins is a leucosome (roughly horizontal) cross-cutting smaller leucosomes which may be evidence for mobilization of melt and accumulation. B) Blocks and rafts of mafic material (*schollen*) in the leucosome of a particularly felsic host. The mafic portions are completely disaggregated. Immediately to the left of the lens cap there is a small proportion of layered migmatite (probably mesosome).

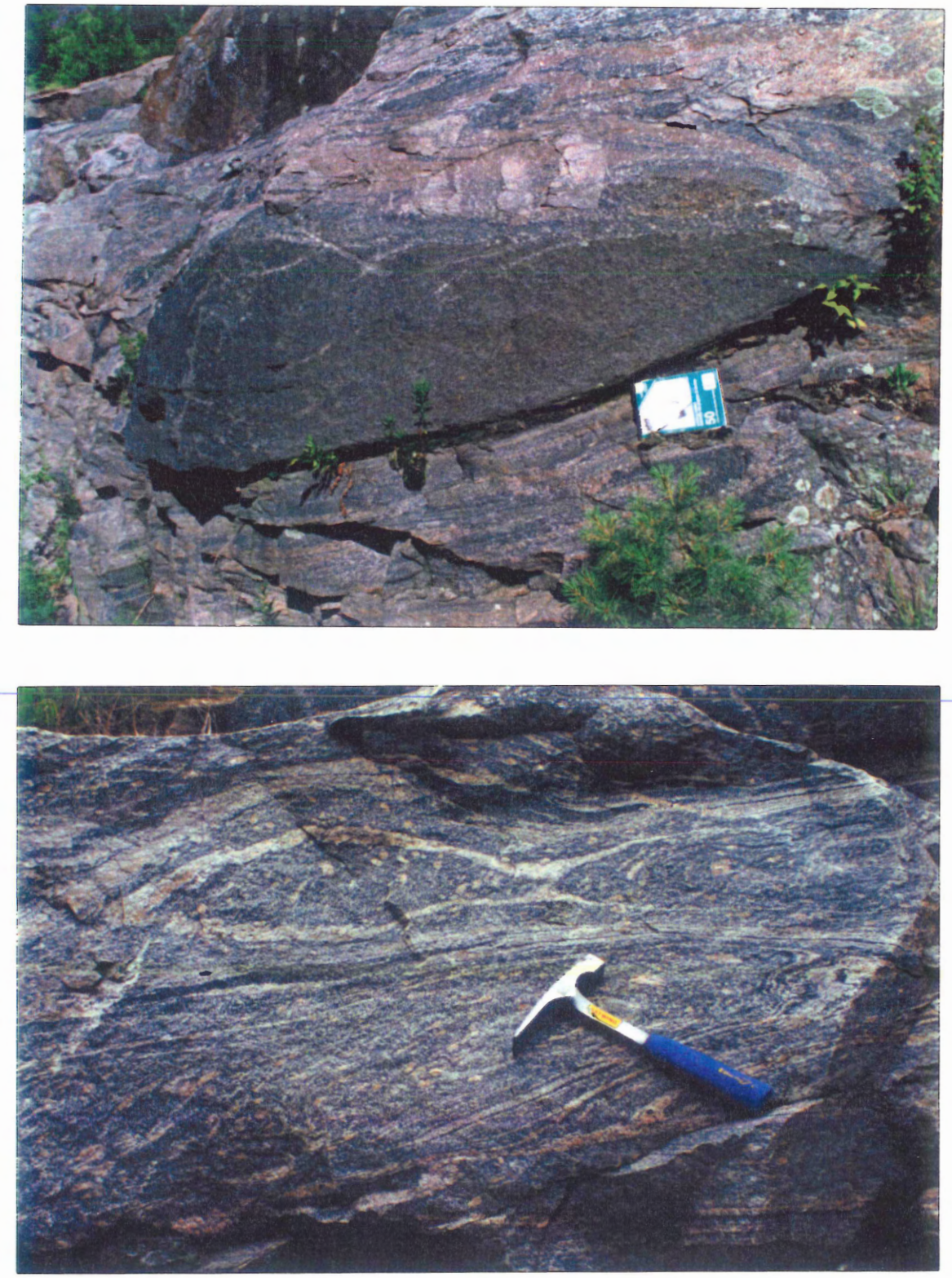

Figure 2.4. A) Mafic enclave 1.5 m wide in stromatic migmatite. The layers of the migmatite wrap around the enclave. In this photograph the leucosome typically cross-cuts the layering giving the rock a wavy appearance. B) Light grey leucosome accumulates in boudin necks, and as small patches throughout the host. The protolith of the patchy leucosome may have been megacrystic.

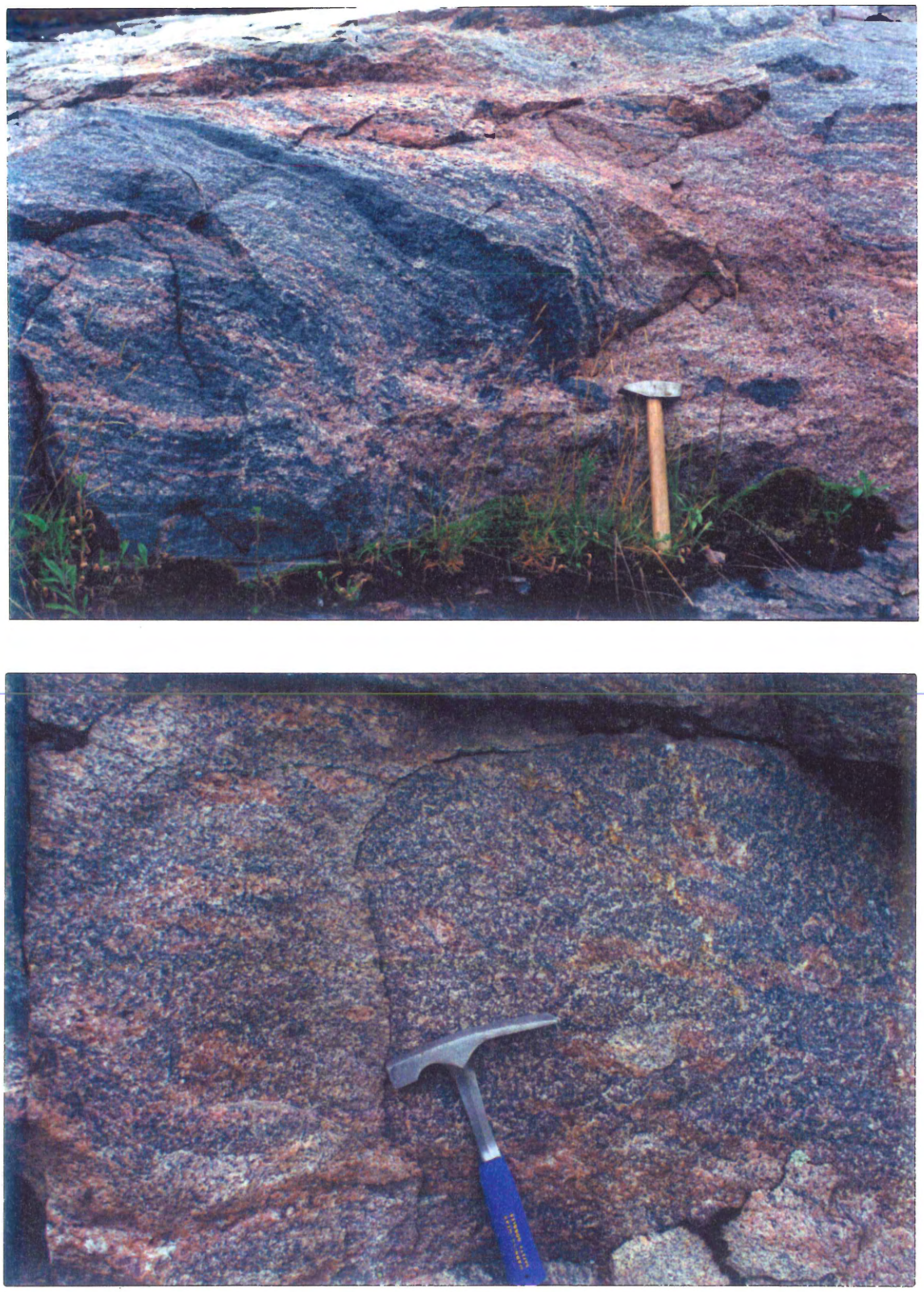

Figure 2.5. A) Relatively large diffuse leucosome cuts mesosome with with small leucosome layers and a mafic amphibolite layer. Small mafic block in leucosome immediately to the right of the hammer. B) Pink leucosome occurs as small patches within the mafic host. This is typical of the dark host litholigies. No layering is present in this area.

variety of rock types. An exceptionally large leucosome cross-cutting the foliation is 3 m in length and 45 cm thick at its centre, pinching out at its ends (Fig. 2.6). The leucosomes are generally coarser-grained than the surrounding rock. Porphyroblasts of hornblende and biotite are equally abundant in leucosomes and surrounding rocks; however they are not present everywhere.

There is no systematic variation between lithology and minor structures in these outcrops (Fig. 2.7). In as short a distance as 5 m there can be a change from planar fabric to convoluted layers to mafic host rock with small patches of leucosome.

2.3 Classification and Hand Sample Characteristics

Samples marked BV- were taken from three laterally adjacent outcrops west of Baysville, Ontario on Highway 117 (Fig.1.1). Samples 95- and 97- were collected by Dr. R.A. Jamieson from the same outcops with one exception; 97-10 was taken from Highway 11 south of Bracebridge, Ontario. In total, 38 samples were chosen to represent the wide range of host rocks and migmatite varieties present. One half of a slab from most samples was stained with cobaltinitrate, which turns the potassium feldspar bright yellow and turns the plagioclase feldspar chalky white (Appendix A).

The samples have been divided into 4 types based upon their macroscopic characteristics. A description of each type follows, and short hand sample descriptions appear in Table 2.1. Type 1 is characterized by non-migmatitic, typically fine-grained, mafic rocks (Fig. 2.8). The samples came from several discrete layers within the migmatites. One sample is a granulite, whereas the other samples are amphibolites that have been intruded by non-migmatitic felsic material. Types 2 through 4 represent varying types of migmatite, based on

Figure 2.6. Largest leucosome in study area, cross-cutting the layering: 0.5 m maximum width and 2.5 m maximum length. Along the periphery of the large leucosome are smaller ones joined to it, similarly cross-cutting the layering. The host rock is of a more mafic variety with thin pin-striped leucosomes.

Figure 2.7. An example of the proximity of very different structural features. Isoclinal folding of the leucosome-rich stromatic migmatites in the upper portion of the photograph. Immediately beneath it are schollen and schleiren type migmatite.

Figure 2.8. Two samples characteristic of the non-migmatitic Type 1 rocks; sample 95-1 on left and sample 97-9 on right.

Figure 2.9. Three Type 2 migmatite samples showing range of host lithologies and leucosome patches. One half of each sample has been stained turning the potassium feldspar yellow and the plagioclase chalky white. From left to right: samples BV-17, BV-5, and 97-4B. Each sample demonstrates a different leucosome variety, however the staining reveals the potassium feldpsar concentration in the leucosomes.

percent and mineralogy of leucosome. Type 2 is the least changed from its protolith, and Type 4 is the most well-developed migmatite.

The samples from Type 2 have the widest variety of macroscopic characteristics. The patches of leucosome range from ellipsoidal (≤ 1cm diameter) to stringy, parallel to, or cross-cutting the foliation (Fig. 2.9). Similarly, the host rocks represent a wide range of felsic to mafic lithologies. Type 3 migmatites are characterized by a moderately well-developed to strong foliation, like most of the outcrops. These samples are all stromatic migmatites, with leucosomes parallel to foliation and parallel to layering (Fig. 2.10). Leucosome layers range from a few millimeters to greater than 1.5cm thick. Hornblende and/or biotite porphyroblasts are characteristic of the Type 4 migmatites (Fig. 2.11). The leucosomes are generally coarser-grained than the Type 3 leucosomes, and may also be discordant to the strong foliation. Unlike all the other types, two samples have three components: leucosome, mesosome, and melanosome.

Table 2.1 — Hand sample descriptions

Sample	Description
Type 1	
95-1	non-migmatitic mafic granulite, homogeneous, fine-grained
97-9	felsic material intruded the fine-grained mafic rock felsic component: granitic composition, light grey.
BV-6	medium-grained mafic host intruded by light grey, fine-grained felsic material
BV-16	same as BV-6
Type 2	
97-4B	light grey leucosome patches ≤ 5mm, commonly discordant, medium-grained, dark grey mafic host
BV-5	pink leucosome patches ≥ 30mm, and small (≤ 10mm) irregular patches in medium-grained, mafic, mesosome; mafic host
BV-14	light pink "linear" leucosome patches ≤ 5mm, typically several cms long, medium-grained; mafic host
BV-17	light grey ellipsoidal to irregular shaped leucosome patches 5-10mm, typically concordant to the foliation, medium-grained; felsic host
BV-20	stringy leucosome patches, comparably thin (~ 3mm) weak foliation, medium-grained; mafic host

Table 2.1 continued

Type 3	
95-2	light pink leucosomes ≤ 10mm thick, medium-grained, planar foliation, fine-grained mesosome; felsic host
97-5	light pink medium-grained leucosomes 2-15mm wide, concordant leucosomes, strong foliation; mafic host
97-6	light pink wavy coarse leucosome 5-30mm wide, concordant to foliation; medium-grained mesosome; felsic host
BV-9	coarse-grained leucosomes ≤ 30mm, medium-grained melanosome, fine-grained mesosome, strong foliation; intermediate host
BV-10	coarse-grained pink leucosome ≥ 10mm, ~ 95-3 but no porphyroblasts, strong foliation; mafic host
BV-34	similar to 95-2, but weaker foliation
Type 4	
95-3	coarse-grained pink leucosome with elongate quartz ≤ 10mm, porphyroblasts ≤ 10mm; dark grey, medium-grained, foliated melanosome; light grey, fine-grained foliated mesosome
95-4A	strong foliation, hornblende porphyroblasts throughout ≤ 8 mm, pink leucosome ≤ 2cm and coarse grained, medium-grained melanosome
97-7	similar to 95-3 but melanosome and mesosome and finer-grained
97-8	medium- to coarse-grained light pink leucosome concordant to foliation, abundant porphyroblasts in leucosome; medium-grained, strongly foliated mesosome; felsic host
97-10	strong foliation, hornblende porphyroblasts throughout, light pink coarse-grained leucosome ≥ 30mm, commonly discordant, medium-grained melanosome?
BV-1	light pink, medium-grained leucosomes with porphyroblasts ≤10mm; fine-grained mesosome; felsic host
BV-4	coarse-grained leucosomes ≥ 15mm with ≤ porphyroblasts 5mm, elongate quartz ≤10mm; medium-grained mesosome
BV-7	coarse-grained pink leucosomes ≥ 3mm with few porphyroblasts; medium-grained mesosome, strong foliation; felsic host
BV-8	pink leucosomes ≥ 50mm, average grain size 10mm, porphyroblasts ≤ 8mm; melanosome medium-grained; intermediate host
BV-11	medium-grained, light pink leucosomes ≤ 20mm, porphyroblasts; mesosomes slightly finer-grained; felsic host
BV-12	medium-grained, light pink leucosomes ≥ 10mm; strong foliation, mildly wavy, mesosome
BV-15	homogeneous, medium-grained leucosome with abundant porphyroblasts
BV-21	coarse-grained pink leucosome ≤ 30mm, similar to 95-4A with less porphyroblasts; mafic host
BV-30	abundant porphyroblasts in dark pink, medium-grained leucosomes ≤ 30mm, strong foliation in finer-grained mesosome; felsic host
BV-33	medium-grained pink leucosome; fine-grained melanosome, strong foliation; felsic host

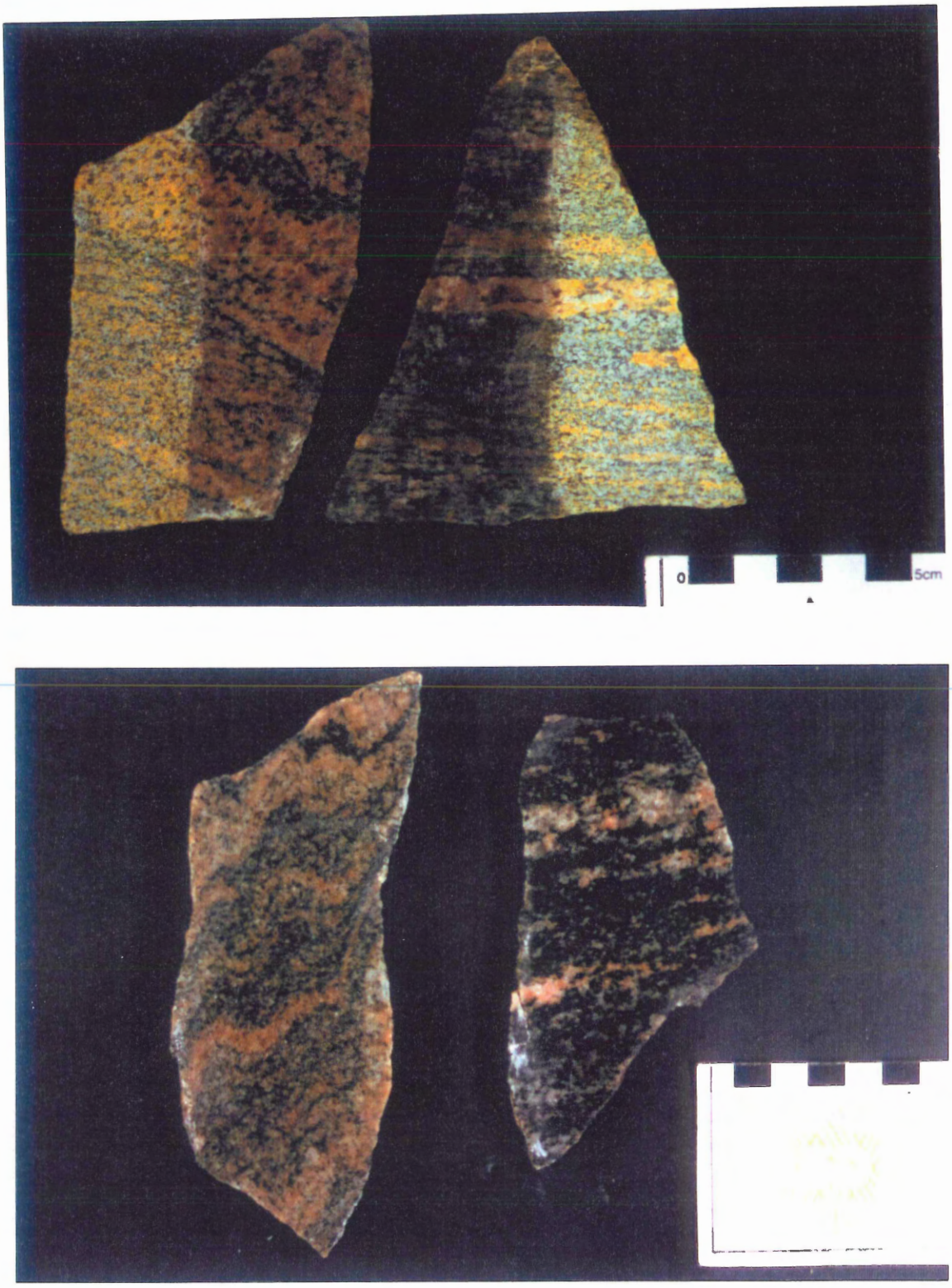

Figure 2.10. Type 3 migmatites. A) One half of each sample has been stained. Sample BV-34 on left, and sample 95-2 on right. The staining reveals the concentration of potassium feldspar in the leucosomes, including the millimeter size leucosomes. B) Sample 97-6 on right has a felsic host and is folded, whereas sample 97-5, has a more mafic host.

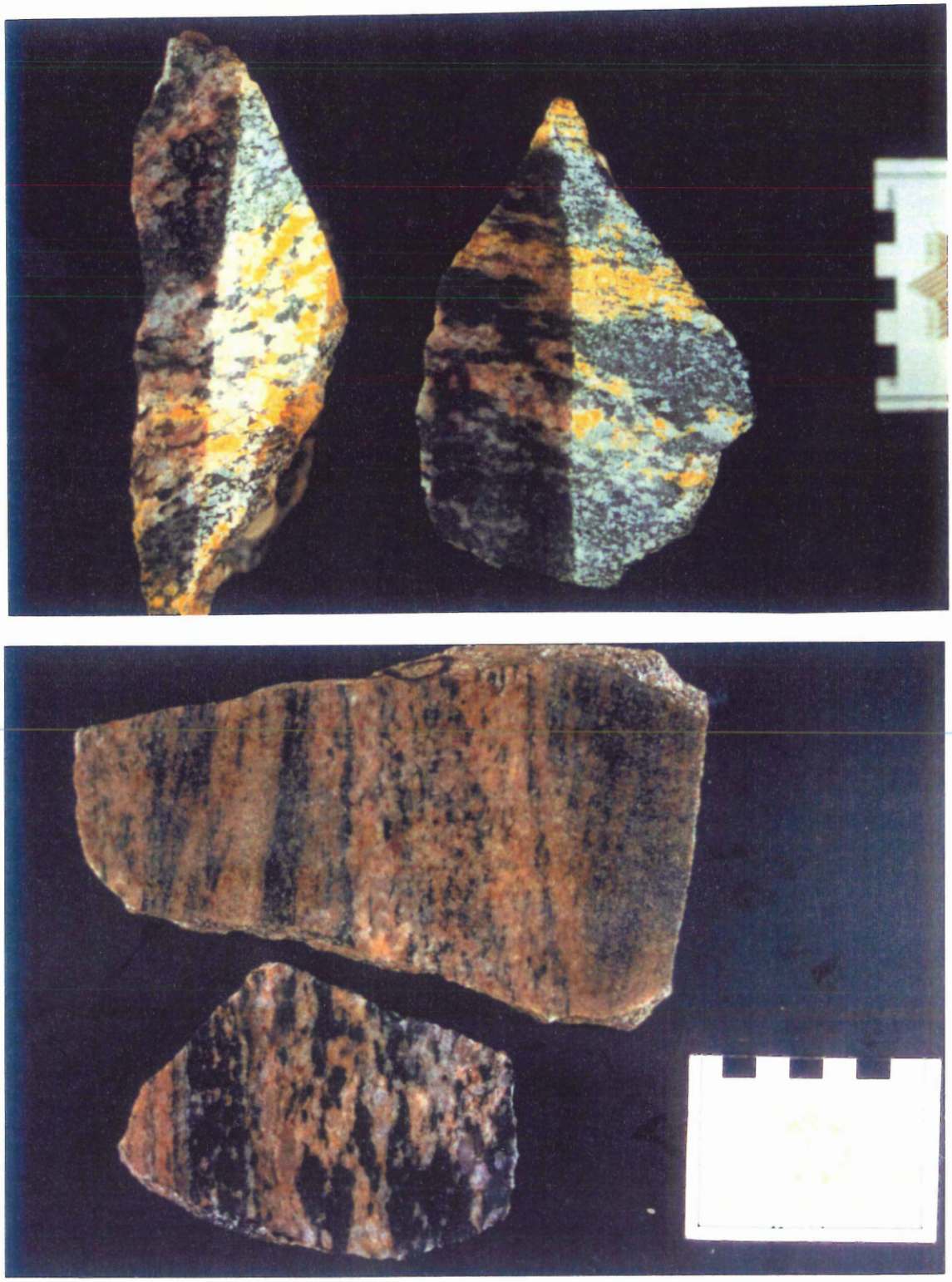

Figure 2.11. Type 4 migmatites. A) One half of each sample has been stained. Sample 97-4A on left, and sample 97-10 on right. The concentration of potassium feldspar in the leucosomes has noticeably decreased relative to Types 2 and 3. Potassium feldspar is rare in the melanosomes. B) Sample 97-8 (on top) has a felsic host, cross-cutting features and small mafic porphyroblasts, whereas sample 97-10 (on bottom) has a melanosome, and large mafic porphyroblasts in cross-cutting leucosomes.

CHAPTER 3 – PETROGRAPHY

3.0 Introduction

This chapter focuses on the petrography of each of the 4 types described in Chapter 2. Twenty-three normal thin sections and 7 large normal sections were examined, and 9 samples were point-counted. Detailed petrographic descriptions and point-counting results are in Appendix B. The purpose of the petrographic study was to examine the textural relationships present in each of the distinct components of the samples, and to note any systematic variations within and between each type.

3.1 Type 1

Non-migmatitic mafic rocks characterize Type 1. The three samples examined have variable mineral assemblages: hb + kf + pl + bt + qz + opq + ap ± opx. Sample 95-1 is a granulite, and contains 11% orthopyroxene, which is in textural equilibrium with the typically larger hornblendes (Fig. 3.1), and locally rims them. The sample is homogeneous, containing approximately 51.3% mafic minerals, and has a granoblastic texture. In contrast, BV-16 has a weak foliation defined by biotite and does not contain pyroxene. Samples 97-9 (Fig. 3.2) and BV-16 have similar mineralogy and textures, however, there are fewer mafic minerals in BV-16, biotite is less abundant and smaller, mosaic texture is less common, and there is greater disparity in grain size in BV-16. Some samples have been injected by non-migmatitic felsic material. Samples 97-9 and BV-16 have similar minerals assemblages: pl + kf + qz + bt + opq + ap + zr. The proportions of quartz, alkali and plagioclase feldspar in

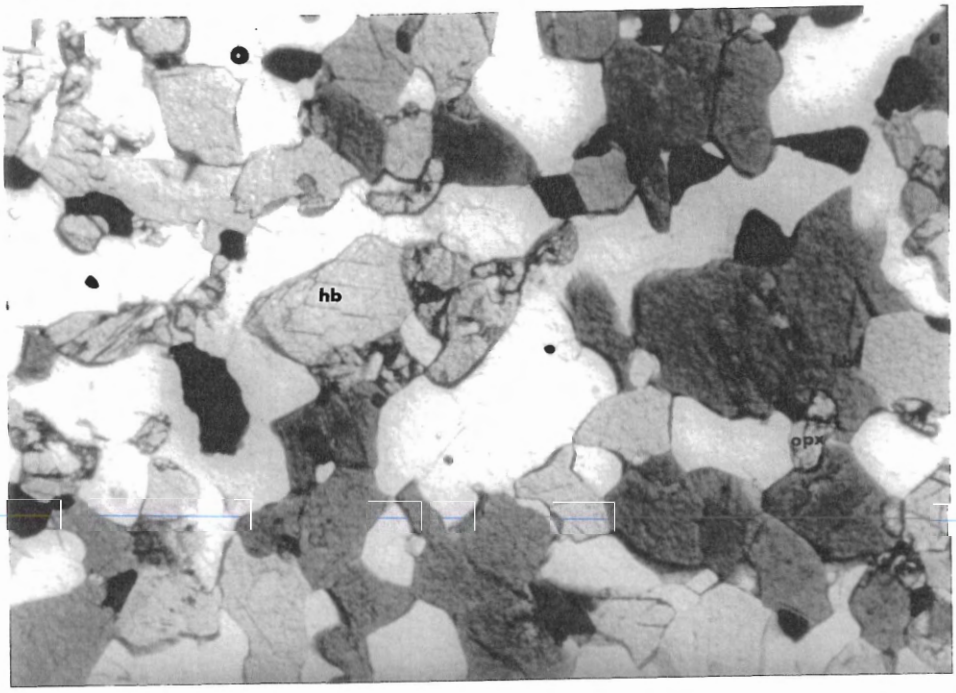

Figure 3.1. Sample 95-1 illustrates a granoblastic texture, with the typically larger hornblende in textural equilibrium with the smaller orthopyroxene. The mineral assemblage is hb + pl + kf + opx + bt + qz + opq + ap. Field of view is approximately 2 mm. PPL.

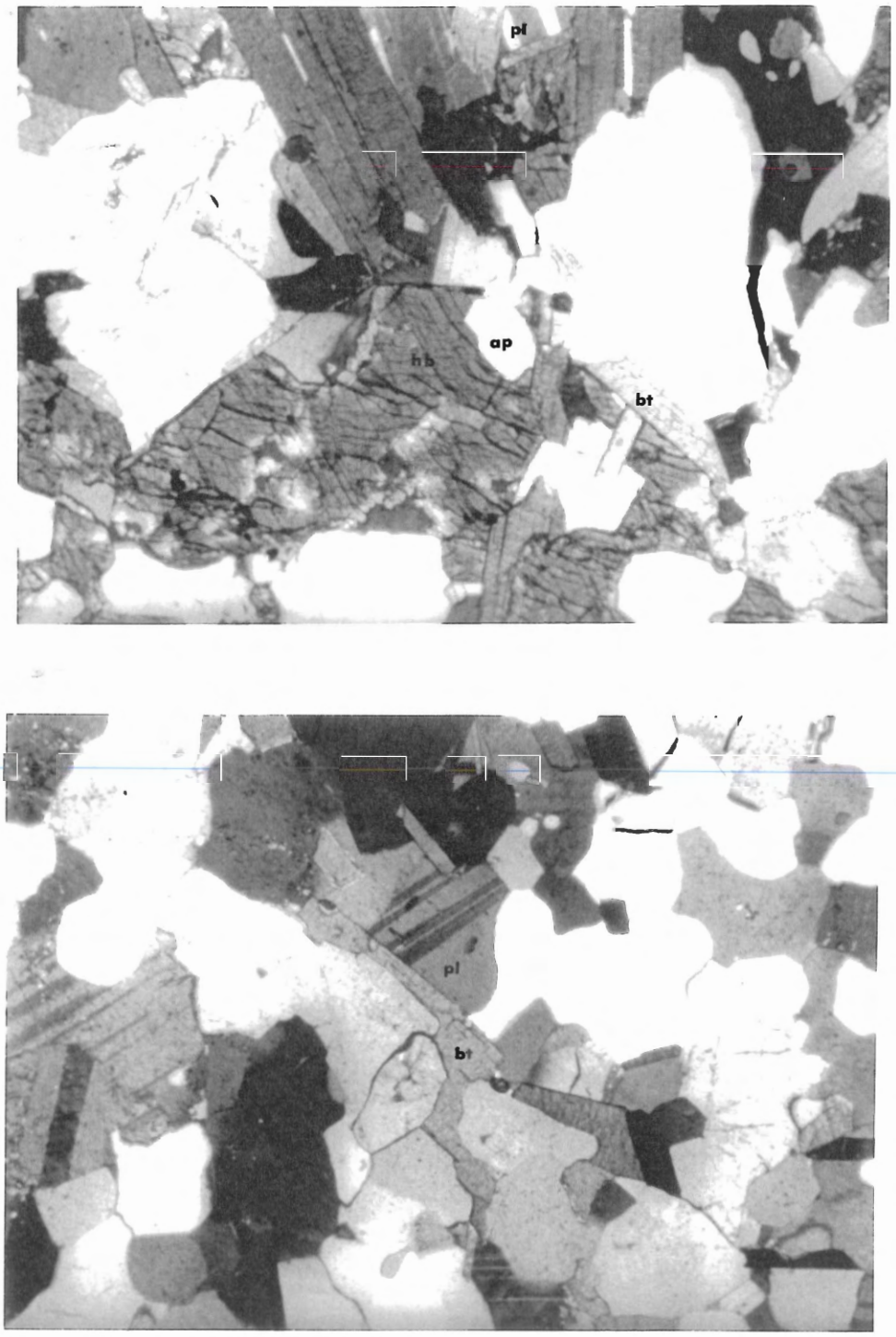

Figure 3.2. Sample 97-9 is typical of the mafic layers within the migmatites. A) The mafic portion is inequigranular with straight to curved grain boundaries. Mineral assemblage is bt + pl + kf + hb + qz + opq + ap. Field of view is approximately 2 mm. XN. B) The felsic portion is inequigranular, however there is a smaller disparity in grain size. Grain boundaries are typically curved, but are also embayed. Mineral assemblage is kf + pl + qz + bt + op + ap. Field of view is approximately 2 mm. XN.

samples 95-1 and 97-9 (obtained by point-counting) are plotted on a QAP diagram (Fig. 3.3).

3.2 Type 2

Type 2 is characterized by stringy, typically thin, discontinuous leucosome patches in a mafic host. The mineral assemblage of a typical matrix (Fig. 3.4) is hb + pl + bt + kf + qz. The percentages of the first four minerals vary considerably, however in all but one case, plagioclase is the dominant felsic mineral. Accessory minerals include opaque minerals, apatite, titanite, zircon, and muscovite. Perthitic feldspar and microcline with cross-hatch twinning are rare (if present) in mesosomes. The grain boundaries are typically curved to straight. The length to width ratio is typically high for biotites in the mesosomes. There are no melanosomes (mafic selvage) present in the samples of this type.

The staining revealed an obvious concentration of potassium feldspar in the leucosome patches in all Type 2 samples (Fig. 2.9). Point-counts yielded extremely high concentrations of potassium feldspar in leucosomes: 65.8% for 97-4B, and 75.0% for BV-17. Modal data from samples 97-4B and BV-17 are plotted on a QAP diagram (Fig. 3.3).

All samples are inequigranular and have curved to embayed grain boundaries. The leucosome patches in each sample are coarser-grained than the adjacent mesosome. The potassium feldspar and quartz porphyroblasts are surrounded by a finer-grained matrix. Mosaic texture in quartz and alkali feldspars, and myrmekite are characteristic of the leucosomes. Microcline with cross-hatch twinning typically constitutes a few percent of each leucosome; however in sample BV-5 (Fig. 3.4) it represents 16% of the leucosomes.

Sample BV-5 can be viewed as a hybrid of Types 2 and 3: it contains small leucosome patches within the mesosome, and one leucosome vein less than 1 cm wide. Although similar

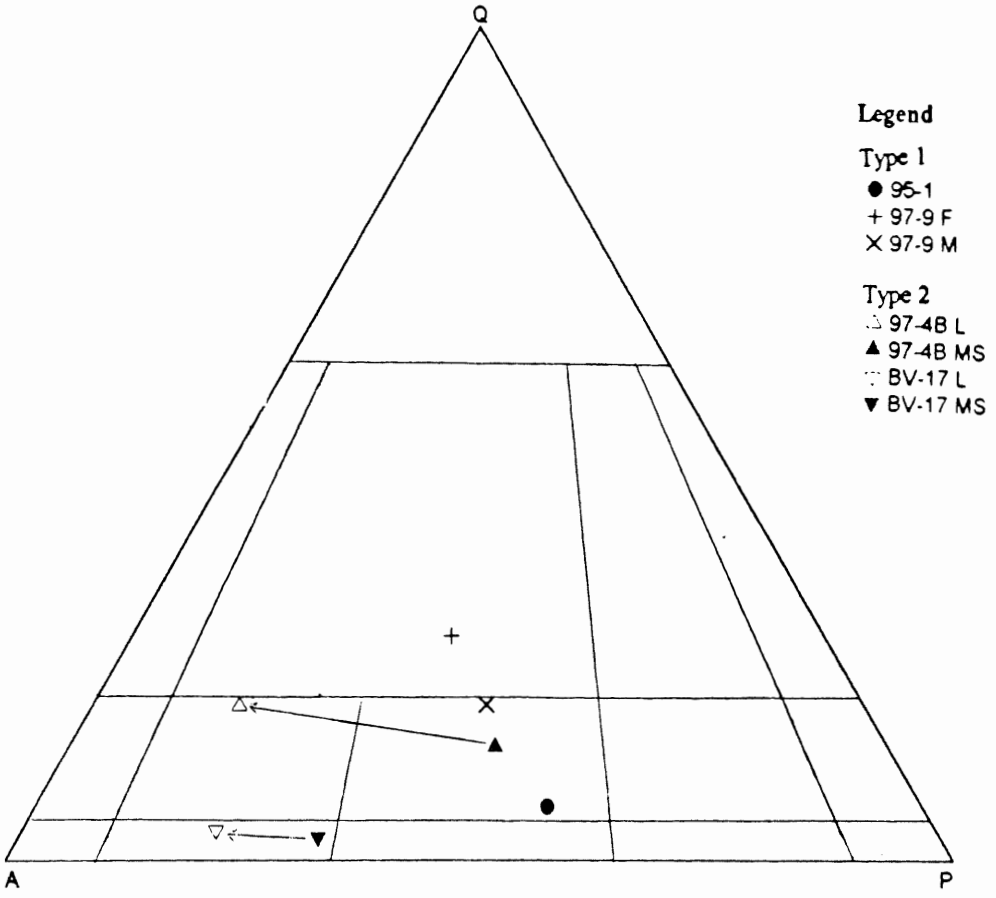

Figure 3.3. Percentages of (Q) quartz, (A) alkali feldspsar, and (P) plagioclase from point-counting results from Types 1 and 2 samples plotted on the IUGS classification of plutonic (phaneritic) rocks. The "x" denotes the mafic portion of sample 97-9, and "+" represents the felsic portion. Open shapes are leucosomes (L), and grey-filled shapes represent mesosomes (MS). Note that the leucosomes plot closer to the "A" apex and the mafic varieties are closer to the "P" apex. Lines with arrows join co-existing leucosome and mesosome.

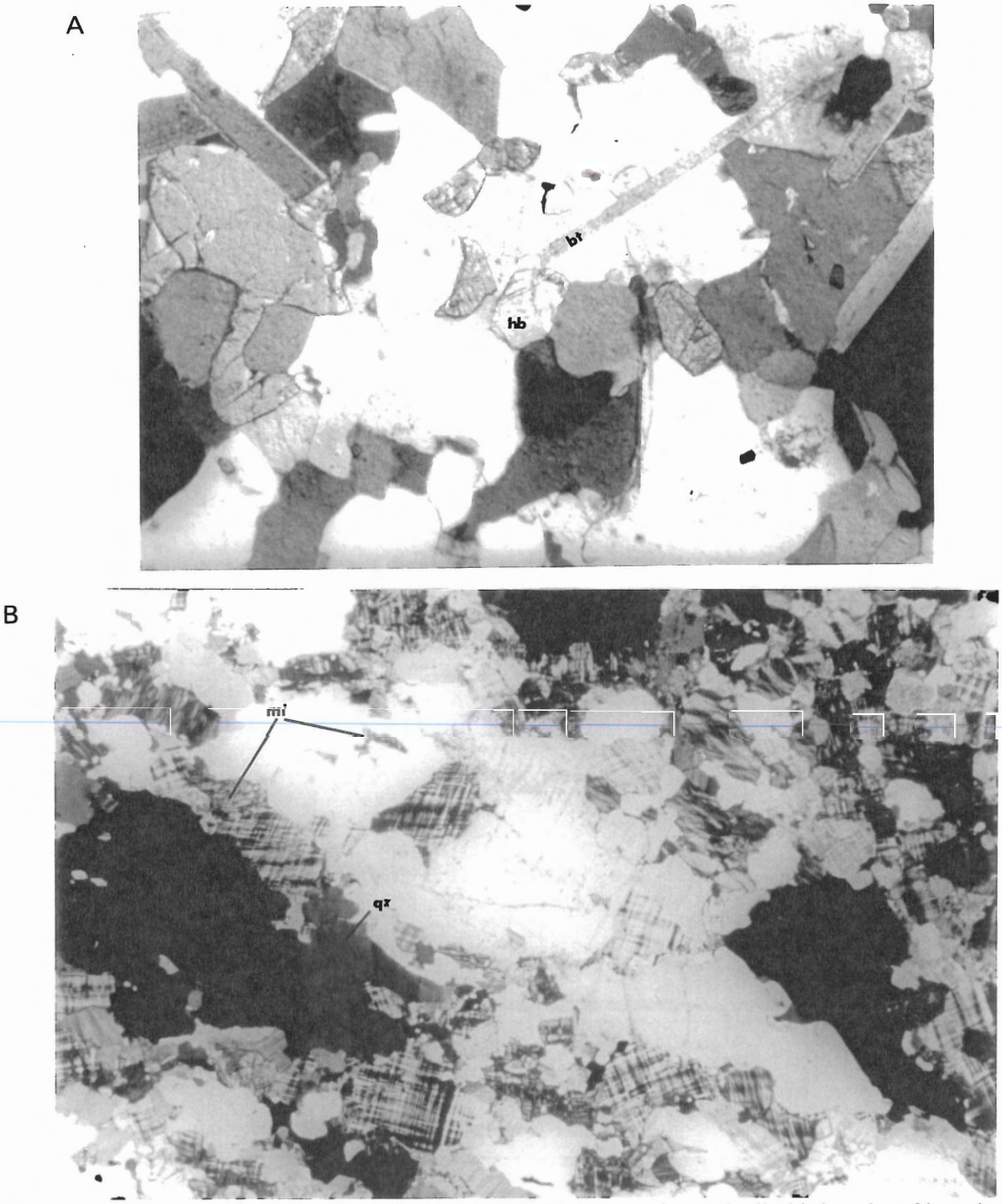

Figure 3.4. Type 2 migmatites. A) Sample 97-4B illustrates the typically high ratio of length to width of biotite grains in mesosomes. Hornblende grains are typically much smaller than the biotite. Mineral assemblage is hb + pl + kf + qz + bt + opq + ap. Field of view is approximately 2 mm. XN. B) Sample BV-17 illustrates the typical texture of leucosomes: porphyroblasts surrounded by a finer-grained recrystallized matrix. Notice the abundance of cross-hatch twinned microcline in the matrix and as inclusions in quartz. Quartz ribbons display undulose extinction. Mineral assemblage is kf + pl + qz. Field of view is approximately 14 mm. XN.

macroscopically, texturally it is quite different from other samples of Type 2, with abundant ≥ 4 cm porphyroblasts of alkali-feldspar (including microcline), and quartz.

3.3 Type 3

Moderately well-developed foliations distinguish the Type 3 migmatites. Plagioclase is the most abundant mineral in the mesosomes of 97-5 (Fig. 3.5) and 97-6. Sample 97-6 has a more felsic composition, there is no hornblende, and the main mafic mineral, biotite, amounts to only approximately 20% of the sample. Conversely, potassium feldspar is the most abundant mineral in sample 95-2. The latter may be due to the probability that point-counting included some of the millimeter-size leucosomes. It plots as a granite on the QAP diagram (Fig. 3.6). The grain boundaries are generally straight to curved, however the felsic minerals in sample 97-6 are typically embayed. Subgrain boundaries in quartz and alkali feldspars are rare, as are myrmekite, perthite, and microcline with cross-hatch twinning.

The leucosomes of all three samples are similar, showing a concentration of potassium feldspars relative to the mesosome. Textures observed in thin section are comparable to those of Type 2; the amount of myrmekite increases relative to Type 2 samples, as does the abundance of subgrain boundaries in quartz and alkali-feldspars in the leucosomes. There is a greater disparity in grain size between the leucosome and the mesosome than in Type 2, with coarser-grained leucosomes. Porphyroblasts of quartz and alkali feldspars are more abundant. The grain boundaries are all curved to embayed, and the samples are inequigranular. The relative proportions of minerals in the leucosomes vary from sample to sample. In all samples potassium feldspar comprises over 40% of the thin section. Perthitic feldspar is more abundant than in Type 2, but is still minor (Fig. 3.5). However, microprobe

A

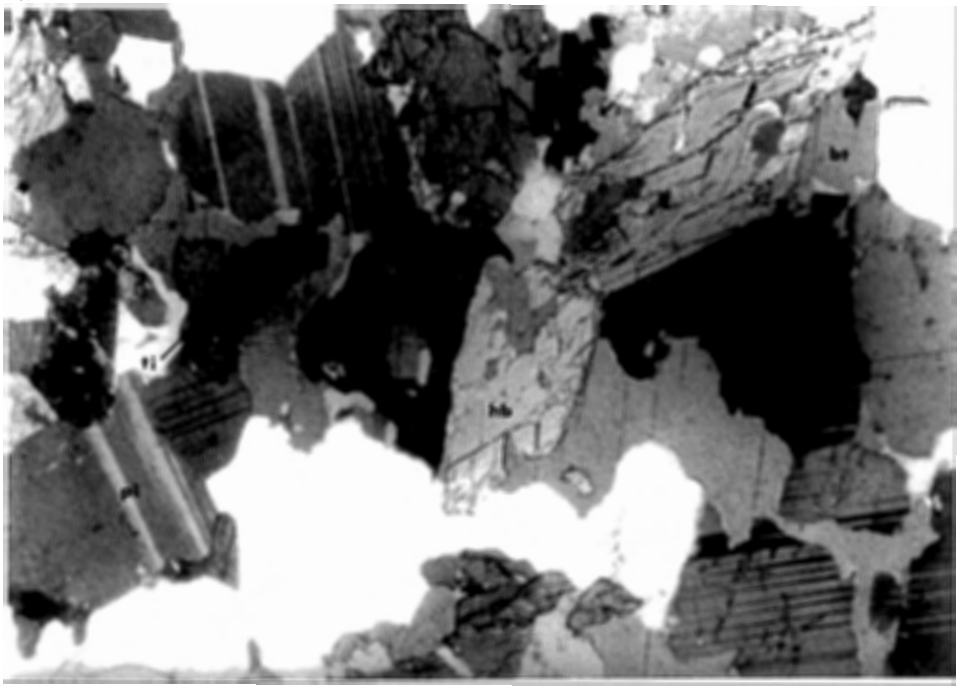

B

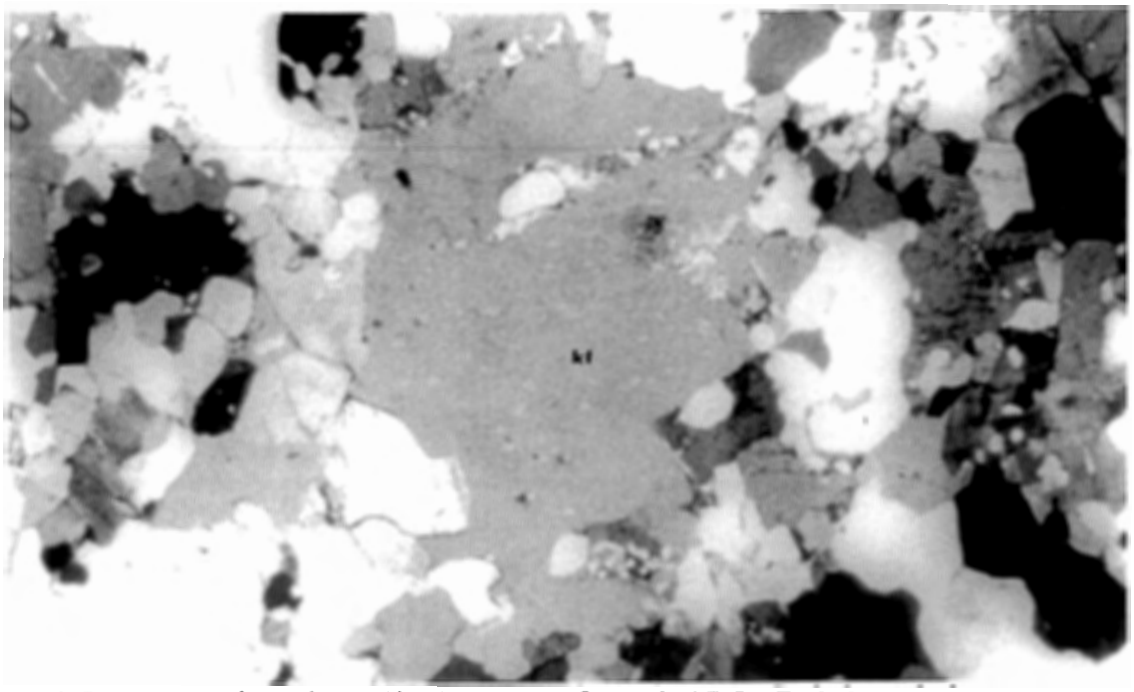

Figure 3.5. Type 3 migmatites. A) Mesosome of sample 97-5. Grain boundaries are typically curved to embayed and the sample is inequigranular. The length to width ratio is close to one for biotite, in contrast to the high ratio observed in Figure 3.3A. Titantite locally rims the opaque minerals. Plagioclase is the most abundant felsic mineral in this sample, and most other mesosomes. Mineral assemblage is pl + hb + bt + kf + qz + opq with ti + zr + ap. Field of view is approximately 3 mm. XN. B) Leucosome from sample 97-6 illustrating the extent of perthitic exsolution typical of leucosomes. Immediately below the perthitic feldspar porphyroblast is myrmekite. Mineral assemblage kf + qz + pl with ap. Field of view is approximately 6 mm. XN.

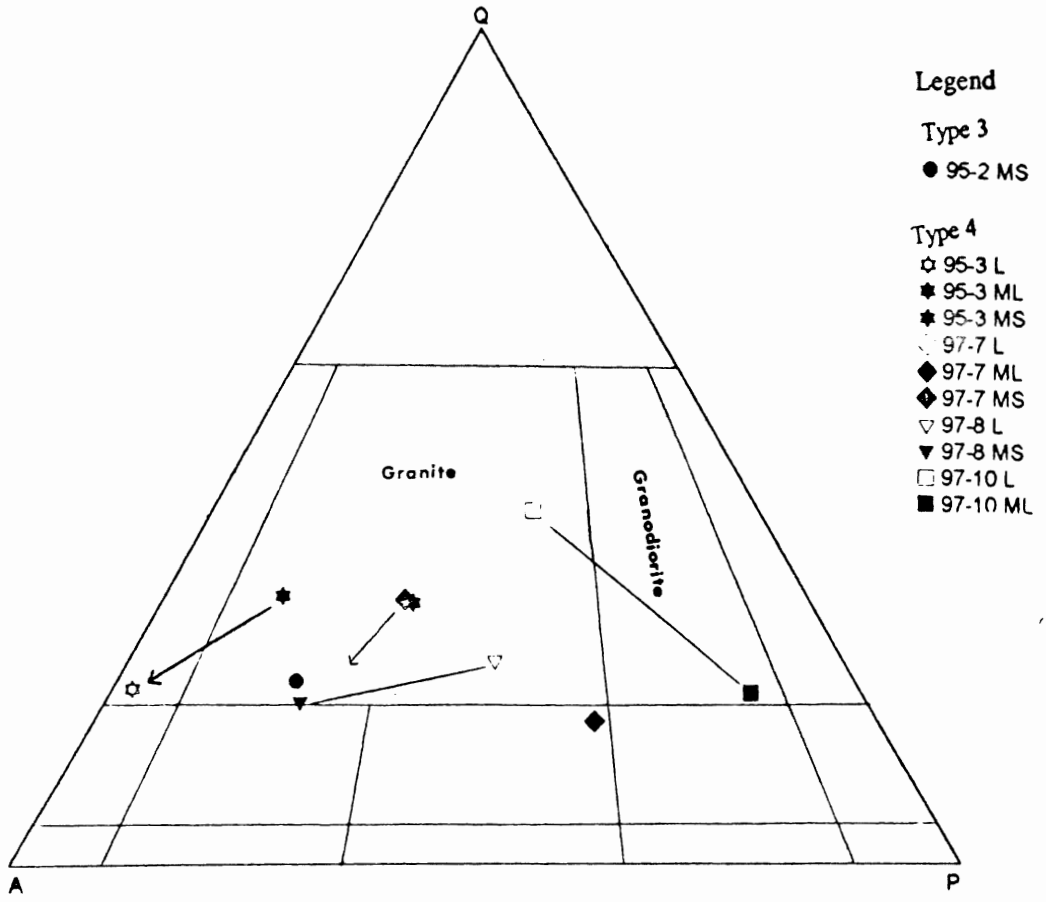

Figure 3.6. Percentages of quartz, alkali feldspsar, and plagioclase from point-counting results from Types 3 and 4 samples plotted on the IUGS classification of plutonic (phaneritic) rocks. Open shapes are leucosomes (L), and grey-filled shapes represent mesosomes (MS), and black-filles shapes are melanosomes (ML). Like the plots for Type 2, the leucosomes plot closer to the "A" apex compared to their respective mesosome and/or melanosome. Sample 97-8 is an exception, the data is probably unrepresentative. The mesosomes of types 95-3 and 97-7 plot have intermediate compositions between their respective leucosome and melanosome. Lines with arrows join co-existing leucosome with mesosome or melanosome.

data (Chapt. 4) suggest that there may be a lot of cryptoperthite within most of the samples.

3.4 Type 4

The migmatites of Type 4 are defined by strong foliation in mesosomes, and hornblende and/or biotite porphyroblasts in the leucosomes. The mesosome of 97-8 (Fig. 3.7) represents a more felsic host, hornblende is rare; this sample is similar to the mesosome of 95-3 and the Type 2 migmatite sample 95-2. The mesosome of 97-7 has more hornblende, and like the others of this type, its boundaries are curved to embayed. Samples 95-4A and 97-10 do not have mesosomes.

The melanosomes of 97-4A and 97-10 are comparable. They both exhibit granoblastic texture and have curved boundaries (Fig. 3.7). The only obvious difference is that the latter is slightly coarser-grained. Samples 95-3 and 97-7 have approximately 20% fewer mafic minerals than 97-10, and potassium feldspar comprises 20% of the melanosome. Samples 95-3 and 97-7 are also finer-grained and the foliation is much better defined in thin section than in 95-4A or 97-10.

The leucosomes of samples 95-3, 95-4A, 97-7, 97-8, and 97-10 are extremely similar macroscopically and microscopically. Like Type 3 leucosomes, all samples except 97-8 show an enrichment in alkali-feldspar relative to their adjacent melanosome or mesosome. In addition, biotite is the dominant mafic porphyroblast, in contrast to hornblende being the most abundant mafic porphyroblast (Fig. 3.7) in the rest of this type. Mosaic texture in quartz and feldspars becomes increasingly characteristic of leucosomes relative to the other migmatite types, myrmekite is more abundant, and the amount of perthitic feldspars and cross-hatch twinning in microcline increases. Quartz ribbons are also increasingly characteristic of the

A

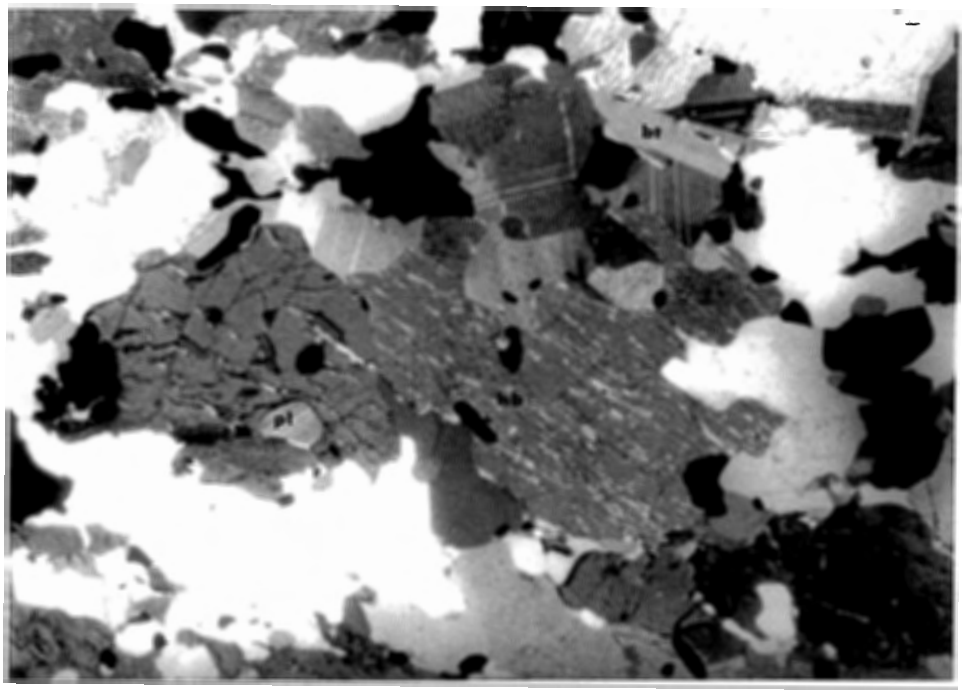

B

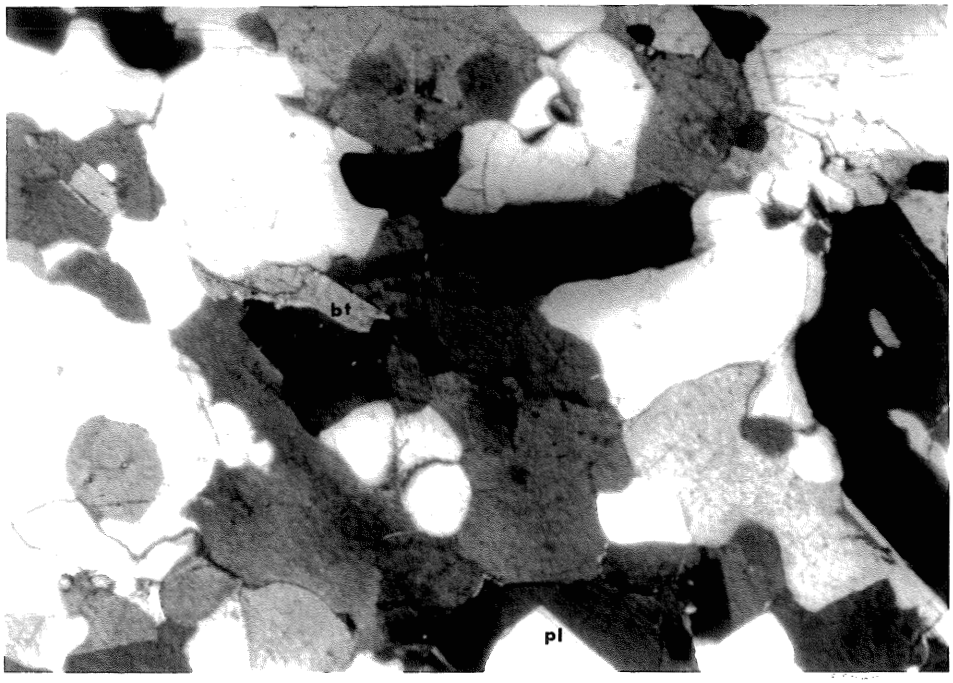

Figure 3.7. Type 4 migmatites. A) Sample 97-8 illustrates the habit of the biotite grains, similar to sample 97-5 with length to width ratio close to one. Mineral assemblage kf + pl + qz + bt + opq + hb w ti + ap + zr. Field of view is approximately 2 mm. XN.
B) Inequigranular melanosome from sample 97-10. Mineral assemblage is hb + pl + qz + bt + opq + kf with ap. Field of view is approximately 7 mm. XN.

C

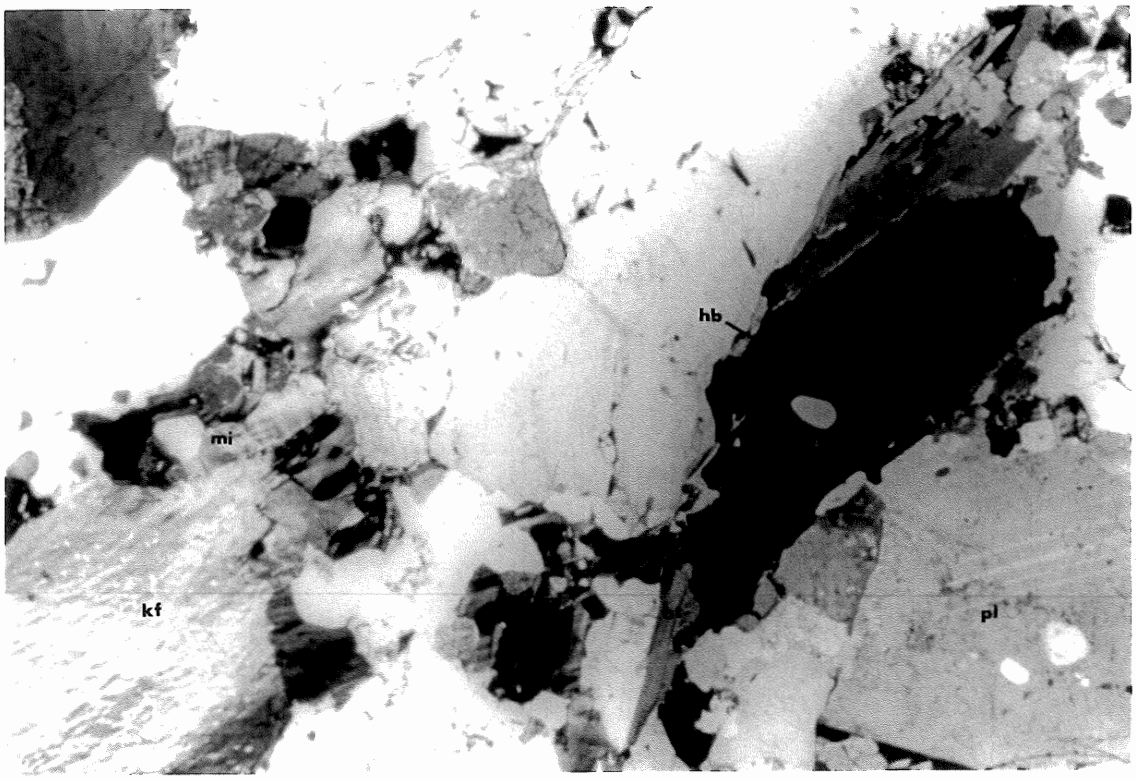

Figure 3.7. C) Hornblende porphyroblast associated with biotite in leucosome of sample 97-4A. Perthite exsolution extensive in feldspar in southwest corner. Round quartz inclusions in plagioclase. Finer-grained cross-hatch twinned microcline surrounding porphyroblasts. Mineral assemblage is kf + pl + qz + hb + bt with opq. Field of view is approximately 14 mm. XN.

migmatites are associated with greater deformation.

Samples 95-3, 97-7, 97-8, and 97-10 are plotted on a QAP diagram (Fig. 3.6). All leucosomes are more granitic than their respective mesosome and/or melanosome, except sample 97-8, where the results are questionable due to the optical similarity of potassium feldspar and quartz grains. Furthermore, the mesosomes plot with compositions intermediate between leucosome and melanosome

3.5 Summary

Type 1 represents non-migmatitic mafic samples. The felsic and mafic portions are present in most samples. The mineralogy of all mafic parts is consistent, hb + bt + pl + kf + qz + opq + ap, and sample 95-1 contains orthopyroxene. All mafic thin sections approach a granoblastic texture. The felsic portions are similar, with mineral assemblage: pl + kf + qz + bt + opq + ap + zr.

The main difference between the mesosomes of all three migmatite types is one of modal percentages. As mentioned, the mesosomes of 95-2 (Type 2) are comparable to 95-3 and 97-8 (both Type 4). All samples contain variable proportions of hb + bt + pl + kf + qz+ opq ± ap ± zr. The major modal differences are between hornblende and biotite. All samples typically have straight to curved boundaries.

Only 3 samples examined have melanosomes, all from Type 4. All are granoblastic, and rich in hornblende, biotite and opaque minerals. They also contain both plagioclase and potassium feldspar, and quartz.

The migmatites of Types 2, 3, and 4 have quite similar leucosome textures compared to melanosome or mesosome. Leucosomes are characterized by porphyroblasts of quartz and

alkali feldspar with rounded inclusions of feldspar and quartz, surrounded by a finer-grained recrystallized matrix. Vernon (1998) suggests that this is characteristic of K-feldspar growth from liquid. Mosaic texture in quartz and feldspar becomes increasingly characteristic of the more strongly foliated migmatites, as do myrmekite, perthite and microcline with cross-hatch twinning. These characteristics are also indicative of higher strain. A concentration of potassium feldspar is observed in most leucosomes, and is typically the most abundant mineral in them. Quartz amounts to 3-20% of the Type 2 and 3 leucosomes, however it becomes dominant in Type 4, amounting to 34% of sample 97-10. Large quartz ribbons ($\leq$ 20mm) occur only in Type 4 migmatites, and there is a trend towards more quartz-rich leucosome with increasing percentage of leucosome.

CHAPTER 4 – MICROPROBE ANALYSIS

4.0 Introduction

The chemical compositions of plagioclase, potassium feldspar, hornblende, biotite, pyroxene, and opaque minerals (magnetite and ilmenite) were determined by microprobe analysis of 8 samples: 95-1, 95-2, 97-4B, 97-7, 97-8, 97-9, 97-10, and BV-17. Some potassium feldspars were also examined for chemical zoning. The results are tabulated in Appendix C. Analysis was undertaken to determine compositional differences in minerals between respective leucosome and matrix, and between different samples.

4.1 Plagioclase Feldspar

All plagioclase feldspars have a narrow compositional range: $An_{21.9\text{-}27.4}Or_{0.2\text{-}3.0}$; with the exception of the non-migmatitic granulite sample 95-1 with $An_{44\text{-}45}Or_{0.2}$. The compositions are predominantly oligoclase (Fig. 4.1), with the exception of sample 95-1 which plots as andesine. Plagioclase is generally normally zoned: 97-10-3 has $An_{26.9}$ in the core, $An_{25.5}$ in the rim; 97-10-4 has $An_{25.8}$ in the core, $An_{25.1}$ in the rim; BV-17-2 has $An_{24.4}$ in the core, $An_{23.5}$ in the rim. In contrast to the previous examples, the rim of 97-10-2 is more calcic, $An_{25.0}$ in the core, $An_{26.1}$ in the rim. These differences are small, but they appear to be significant within error of microprobe results.

4.2 Potassium Feldspar

The compositions of the potassium feldspars are not as consistent as those of

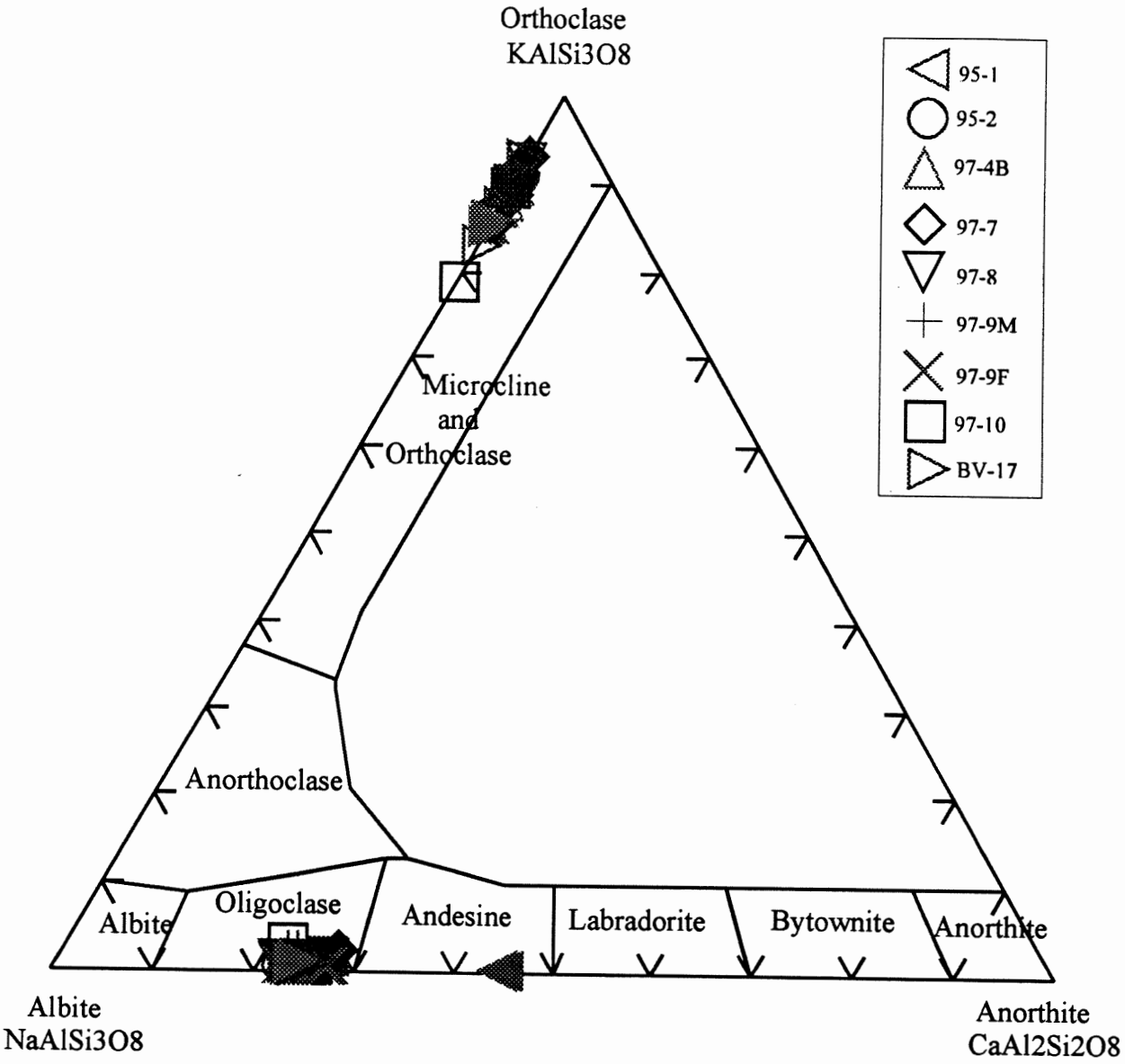

Figure 4.1. Feldspar compositions of all samples plotted on a standard feldspar ternary diagram. Each sample has a different shape; filled shapes represent mesosome or melanosome, and open shapes represent leucosome. Note extremely consistent plagioclase compositions and slightly more variable potassium feldspar compositions.

plagioclase. All samples had $Or_{86-94}An_{0.0-0.7}$. The results are presented in Figure 4.1. The leucosome of sample 97-8 contains potassium feldspar that is more sodic (Or_{85-89}) than potassium feldspar in the coexisting matrix (Or_{91-93}). None of the potassium feldspars examined were chemically zoned. However, perthite exsolution is abundant.

4.3 Biotite

Biotite compositions are generally consistent, with iron–magnesium ratio [Fe/(Fe+Mg)] from 0.4 to 0.6 (Fig. 4.2), except for sample 95-1 which is more magnesian (0.3 to 0.4). The ratio of elements is generally consistent for each sample. However, the percent oxides are variable for FeO (14.75 - 19.05%), MgO (10.77 - 15.11%%), and TiO_2 (2.92 -5.61%).

4.4 Hornblende

Hornblende compositions are generally consistent with magnesium-iron [Mg/(Mg+Fe)] ratio 0.5-0.6 (Fig. 4.3), except 95-1 which is more magnesian (0.6-.0.7). They all plot in the ferroan pargasitic hornblende field. The weight percents that differ by more than 1% are: FeO (15.18 - 18.17%), MgO (9.7 - 11.41%), Al_2O_3 (10.16 - 12.55%), CaO (10.91 - 11.95%), and TiO_2 (1.26 - 2.38%). A leucosome of sample 97-4B has higher magnesium and less iron than in the matrix.

4.5 Orthopyroxene

The non-migmatitic sample 95-1 is the only sample with orthopyroxene. The

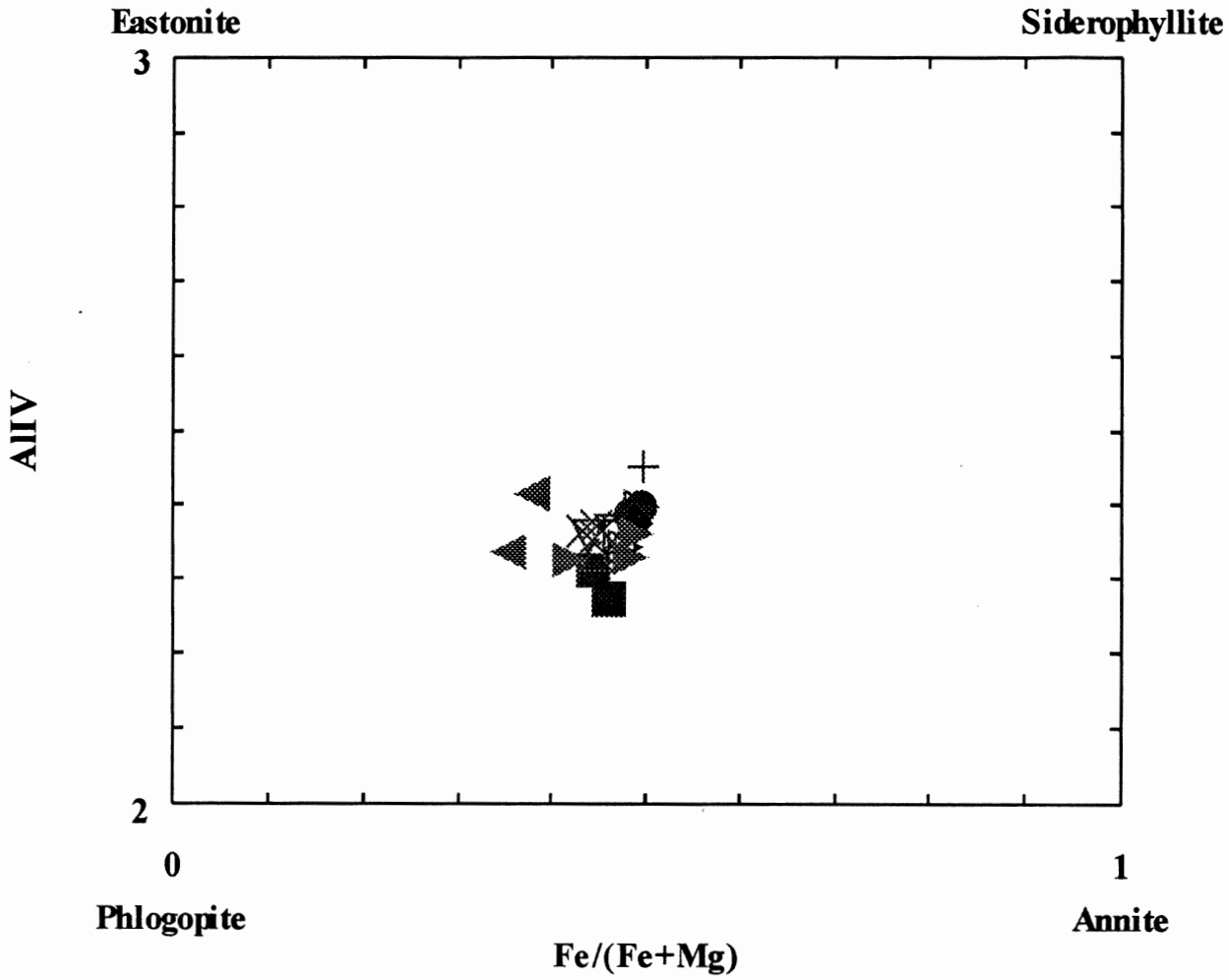

Figure 4.2. Aluminum versus Fe/(Fe+Mg) for all biotites. All calculations based on the assumption that all Fe = Fe^{+2}. If the leucosome formed by partial melting, there might be less Mg in the biotites of the leucosome than in the melanosome or mesosome. Furthermore, there should be lower Fe/(Fe+Mg) in the mesosome and melanosome and in mafic rocks. This is observed in the relatively mafic sample 95-1, with the lowest Fe/(Fe+Mg). Symbols as for Figure 4.1.

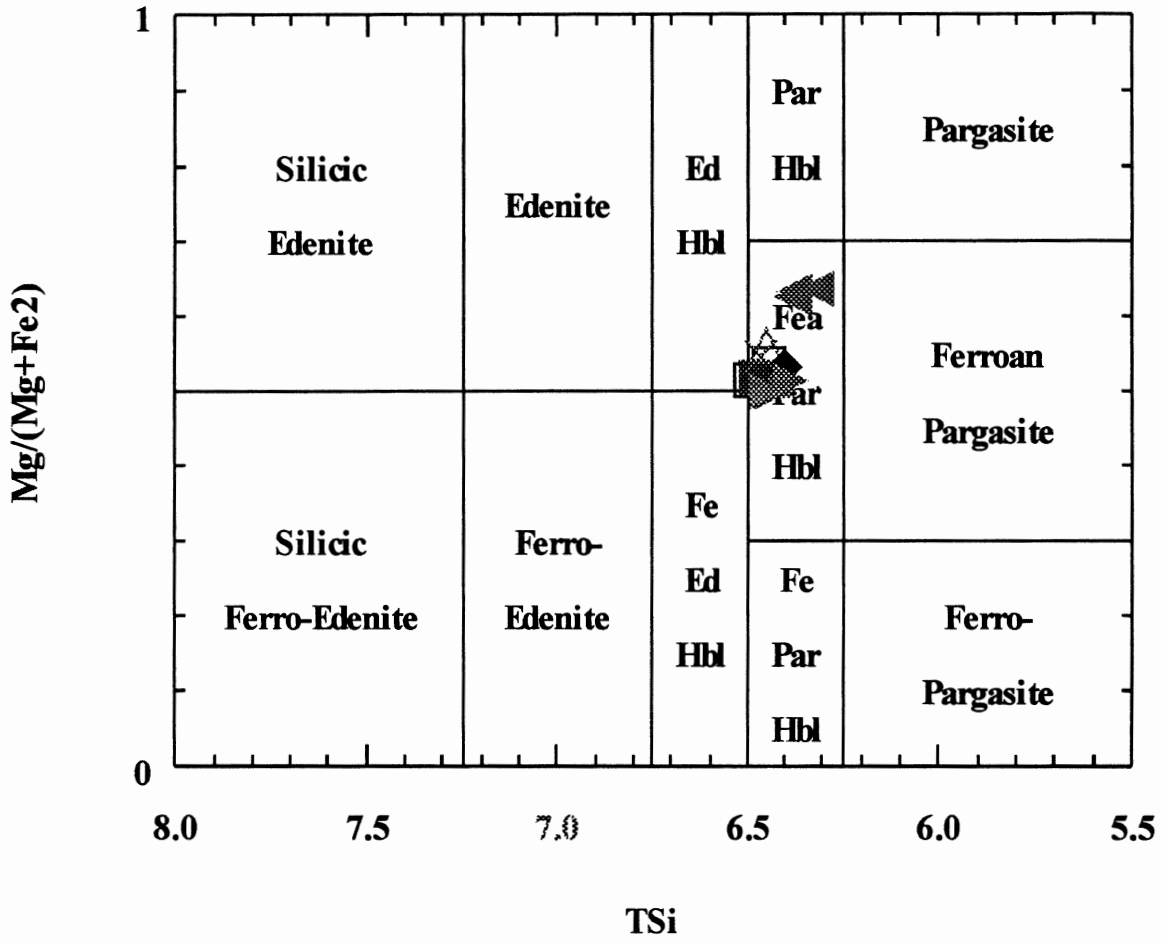

Figure 4.3. All hornblendes plotted on an amphibole classification diagram of $Mg/(Mg+Fe^{+2})$ versus TSi. As noted in Figure 4.3, hornblende in melanosomes and mesosomes should be enriched in Mg relative to leucosomes. Mafic rocks should also have higher Mg. This is observed in 95-1. Symbols as for Figure 4.1.

compositions are uniform, plotting on the orthopyroxene En-Fo-Wo diagram as hypersthene, with En_{55-60} and Fs_{40-45} (Fig. 4.4).

4.6 Opaque minerals

The analyzed opaque minerals in all the samples are zoned. They are all Fe-Ti oxides, belonging to either of two solid solution series: hematite-ilmenite or magnetite-ulvospinel series.

4.7 Summary

Plagioclase feldspars are normally zoned, and have a narrow compositional range: $An_{21.9-27.4}Or_{0.2-3.}$ The compositions of the potassium feldspars are more variable than those of plagioclase. All samples had $Or_{86-94}An_{0.0-0.7}$, and perthite exsolution is abundant. The compositions of biotite and hornblende are generally consistent. All components except FeO and MgO vary by less than 2% weight oxide. If a trend is evident for FeO and MgO between leucosome and matrix (i.e. mesosome or melanosome), the biotite and hornblende in the matrix are enriched in magnesium relative to leucosome. Orthopyroxene occurs only in the non-migmatitic sample, and analyses are uniform. The opaque minerals belong to either the hematite-ilmenite series or magnetite-ulvospinel series.

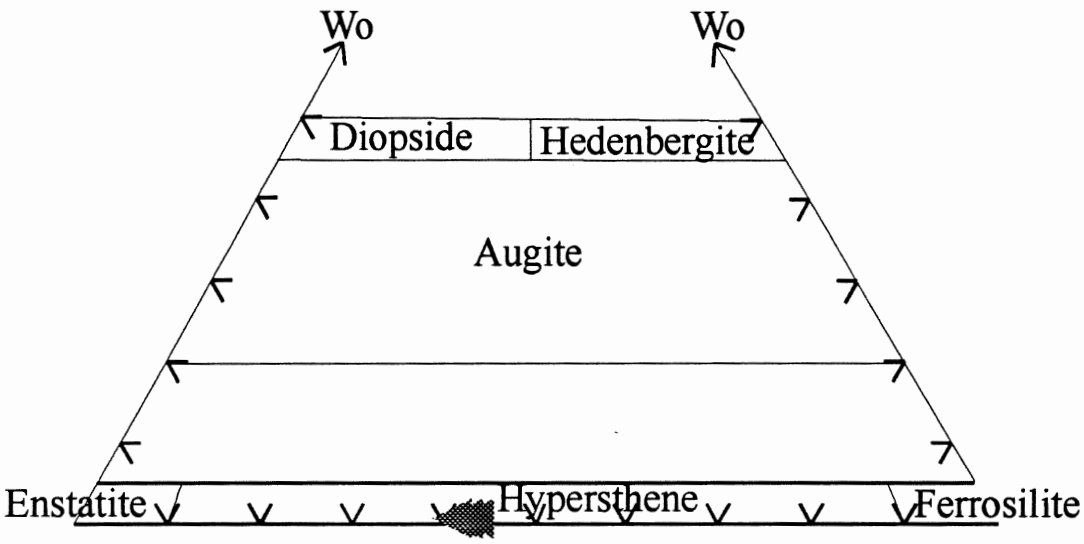

Figure 4.4. Pyroxenes plotted on a wollastonite-enstatite-ferrosilite classification diagram.

CHAPTER 5 - INTERPRETATIONS

5.0 Introduction

This chapter focuses on the petrogenesis of the migmatites of the Muskoka Domain. As discussed in Chapter 1, each of the four possible migmatization mechanisms discussed by Yardley (1978) will be considered, recognizing that more than one process may be responsible for migmatization. These processes are: igneous injection, anatexis, external metasomatism, and metamorphic segregation (internal metasomatism).

5.1 Migmatization Mechanisms

Firstly, hydrothermal processes, which can be considered metasomatic, are discussed. Metasomatism is a segregation process, involving the transport of material through intergranular fluid, which is controlled by chemical potential gradients set up within a compositionally heterogeneous protolith. Although this mechanism has been well documented on an outcrop scale, there is little evidence that internal or external metasomatism is the main mechanism responsible for the development of migmatites on a regional scale (Ashworth, 1985).

Igneous injection may cause migmatization through formation of intrusion breccias. However, no igneous intrusions have been found in the area, therefore this process is extremely unlikely. Furthermore, field relations should be quite different from those observed. Small leucosome patches would not be expected proximal to stromatic migmatites.

Nor would there be abundant diffuse leucosome patches disconnected from any obvious veins or dykes (Fig. 2.5).

In situ anatexis is the last process to be considered as a migmatization mechanism. By the process of elimination, it is the most likely cause; however, all evidence for and against should be considered. Furthermore, it must be established whether the system was open or closed, i.e. did any melt leave the system? Although this is usually done by chemical or mass balance techniques (Nyman et al. 1995) which were not included in this thesis, field and petrographic data can also be used to test this possibility.

Vernon (1998) proposed microstructural criteria for distinguishing between anatectic leucosome and quartz-feldspar aggregates formed in solid-state. If the leucosome is anatectic, it should contain igneous features. More specifically he lists four criteria: (1) idioblastic crystal faces of feldspar may occur against quartz; (2) inclusion trails absent compared to same minerals in the mesosome; (3) overgrowths free of inclusions trails may occur on minerals with inclusion trails; and (4) simple twins may be present in potassium feldspar. Unfortunately, these igneous features may be obliterated by subsequent deformation and recrystallization. This is the case with the study area, being especially evident from the increase in cross-hatch twinning in microcline, and grain boundary recrystallization evident from myrmekite and mosaic texture.

5.2 Equilibrium versus Fractional Melting

Equilibrium melting occurs when the liquid and solid remain in contact and in equilibrium. The first melt produced during melting of a plagioclase-bearing parent rock

should contain plagioclase that is approximately ~10-40% more sodic than the plagioclase in the parent (Fig. 5.1). As the temperature increases, the liquid becomes more calcic until all the solid has melted and plagioclase has the same composition as in the original solid. In the alkali feldspar system (Fig.5.2), the first melt produced from an orthoclase-rich parent contains alkali feldspar that is ≤ 40 % more sodic than in the solid. If the leucosomes were formed by equilibrium melting, small patches of leucosome should contain alkali feldspar that is significantly more sodic than larger concentrations of leucosome.

Fractional melting is the opposite of equilibrium melting. It occurs when the liquid is continually removed from the solid residuum. The composition of the first melt is the same as in equilibrium melting, however since the melt is continually extracted, each successive melt of plagioclase with increasing temperature will be more calcic, until it reaches An_{100} (Fig. 5.1). If the leucosomes formed by fractional melting, the plagioclase in the host should be much more calcic than in the leucosome, and the alkali feldspar should be much more potassic in the host (Fig. 5.2).

5.3 Evidence for Anatexis?

Regardless of the type of melting that occurred, the experimental studies indicate that plagioclase in a partial melt should be more sodic than the residual plagioclase (e.g. Bowen, 1913). Therefore, the average plagioclase compositions of the leucosome compared to the melanosome or mesosome should differ on the ternary diagram (Fig. 5.3). This phenomenon is observed in sample 97-7, which contains An_{24} in a leucosome patch and An_{27-28} in the melanosome. Plagioclase in the leucosome of sample 97-10 is slightly more sodic (An_{22-26}),

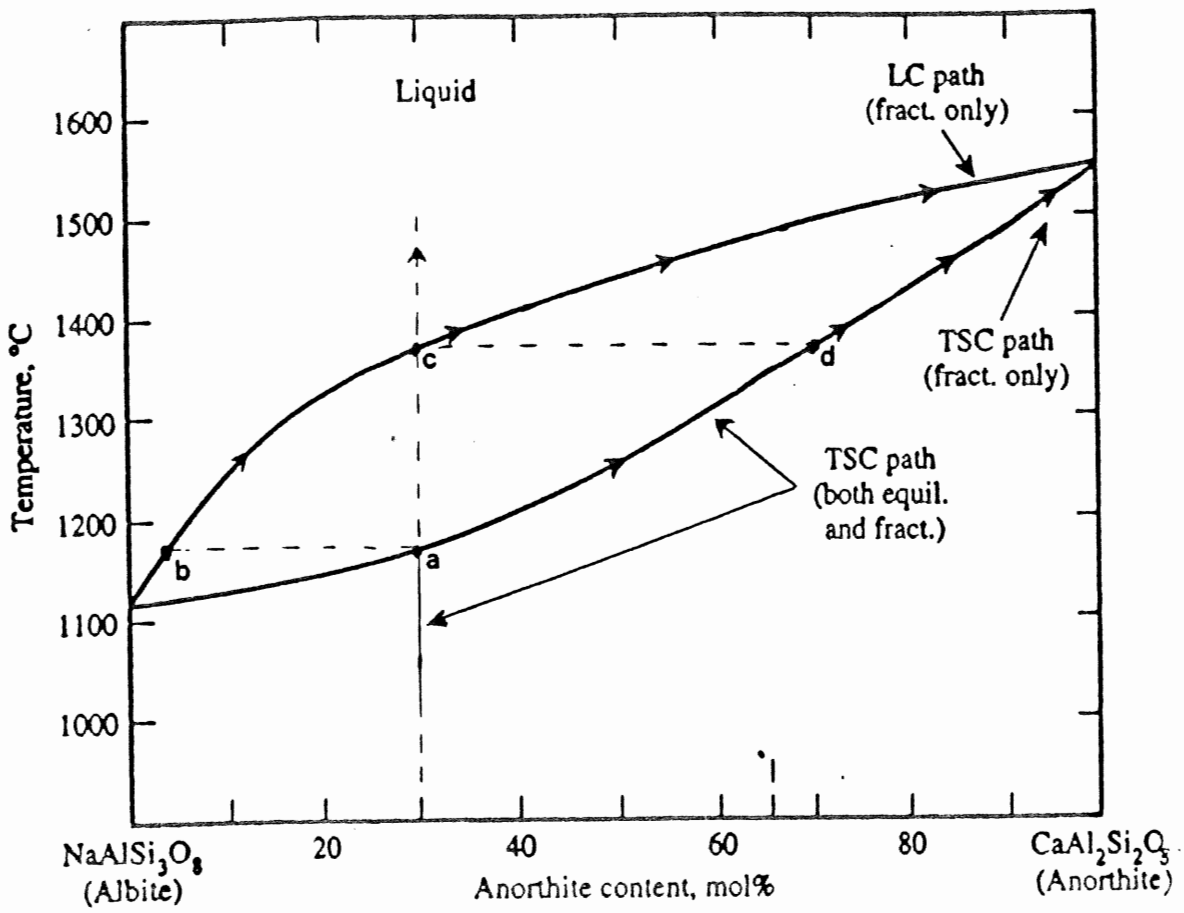

Figure 5.1. Binary system $NaAlSi_3O_8$ (albite) - $CaAl_2Si_2O_8$ (anorthite) showing the total solid composition (TSC) and the liquid composition (LC) paths for equilibrium (equil.) and fractional (fract.) melting. Solid An_{30} is used for an example. For equilibrium melting the first melt will have An_4 (point *b*). As the temperature increases, the percentage of melt increases and the liquid constantly reequilibrates with the solid becoming more calcic. When the composition of the LC equals the composition of the original solid the entire system is molten (point *c*). The last TSC occurs as point *d*. The first melt for fractional melting also forms at point *b*. Since the liquid is continually being removed from the system, the liquid cannot re-equilibrate with the solid, thereby driving the LC and TSC towards the anorthite end member. Ultimately both LC and TSC will be pure anorthite, however, in this example only a small amount of the original volume will remain. Note temperatures are for the simple Ab-An system only. Modified after Blatt & Tracy (1996).

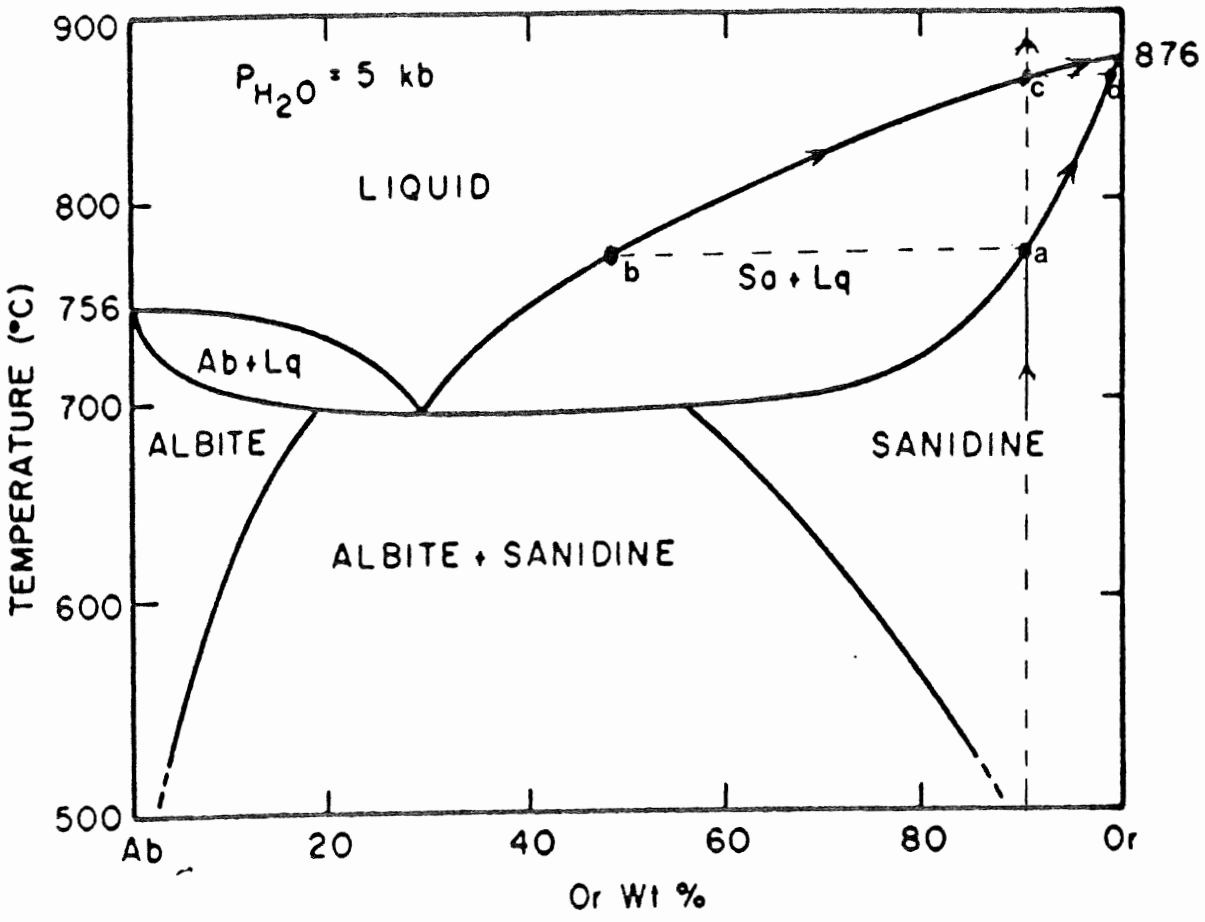

Figure 5.2. Binary phase diagram for the $NaAlSi_3O_8$ (albite) - $KAl_2Si_2O_8$ (orthoclase) system at 5 kb under water saturated conditions. The abbreviations are the same as for Figure 5.1, using a single phase solid of Or_{90} as an example. For equilibrium melting, the LC will follow a similar path to Figure 5.1; first melt appears at point *b* with Or_{50}, becoming for potassic with higher temperature until it reaches the initial TSC at point *c*. The TSC follows a similar path from point *a* to *d*. The first liquid formed by fractional melting also appears at point *b*, continuing to pure orthoclase. Unlike the plagioclase case, with this starting point there should be a substantial portion of the original solid with a final LC of Or_{100}. The TSC also follows the path to pure orthoclase, but starts at point *a*. These temperatures are for a simple Ab-Or system only. Modified after Morse (1980).

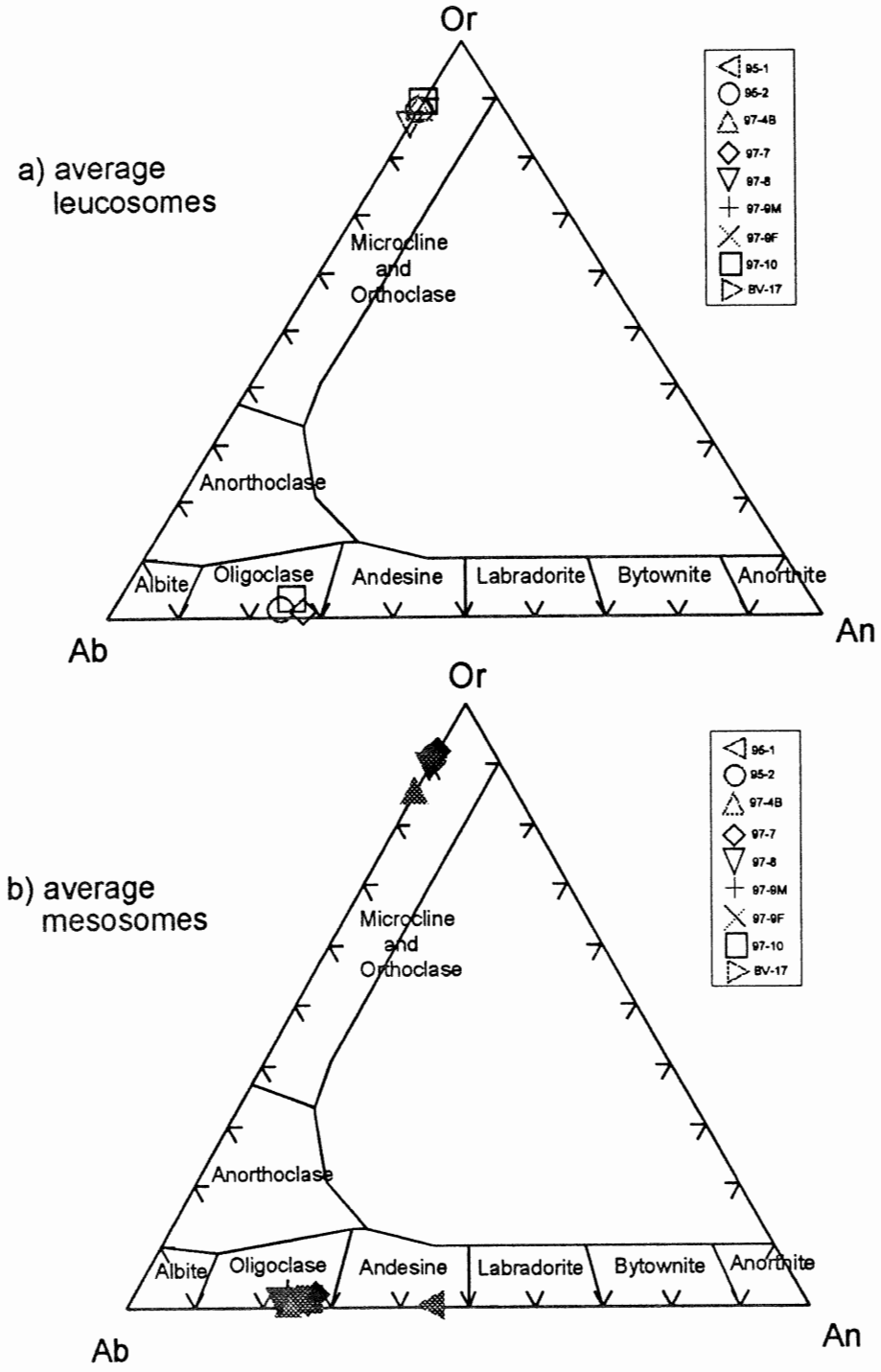

Figue 5.3. Average feldspar compositions plotted for each sample on two diagrams for clarity; a) feldspars from leucosomes, and b) feldspars from mesosomes and melanosomes. If the leucosome formed by partial melting, it is expected that plagioclase in the leucosome will be more sodic than in the mesosome. This is not the case, the average plagioclase and potassium feldspar compositions from the leucosomes are very similar to those in the mesosome.

but overlaps with melanosome plagioclase (An_{26-27}). There was no difference observed between the leucosome and matrix of the other samples. Similarly, potassium feldspars should be more sodic in the leucosome. The potassium feldspars of sample 97-8 are consistent with partial melting, with Or_{91-93} in the matrix and Or_{85-89} in the leucosome.

Yardley (1978) and Misch (1968) suggested that migmatites that do not have more sodic plagioclase in the leucosomes are not anatectic. However, apparently anatectic migmatites are commonly observed to have similar feldspar compositions in the leucosome and matrix. Johannes (1985) suggested that: (1) a second period of metamorphism could homogenize plagioclase compositions; and (2) following crystallization the plagioclase in the leucosome and mesosome could homogenize because they are in "intimate" contact. During equilibrium melting, the melt constantly re-equilibrates with the solid. This re-equilibration could account for the scarcity of sodium-rich plagioclase in the leucosomes in this study. However, a more likely explanation is that since the protolith was an orthogneiss with a granodioritic composition, the composition of the plagioclase feldspars in the protolith was similar to its present composition.

5.4 Pressure and Temperature Estimates Relative to Melting Curves

Pressure and temperature estimates in the Muskoka Domain support an anatectic origin. Timmermann (pers. com. 1998) estimated peak metamorphic temperatures from 753 to 854°C, at pressures from 10.3 to 11.3 kbar. Similarly, in a regional compilation of pressure and temperature data, Anovitz and Essene (1990) reported temperatures of 740 to 875°C, at pressures of 9.8 to 10.5 kbar. The migmatite protoliths were granodiorites and granites,

therefore experimental data on melting and crystallization in the granite system apply directly. Minimum melts in the granite system Qz-Or-Ab-An-H_2O with $An_{\leq 40}$ form at temperatures from 650 to 710°C above 2 kbar; this is well below those estimated for the region (Fig. 5.4). If the protolith was saturated with H_2O at these temperatures and pressures, it would have been entirely molten. This shows that the rocks were substantially above melting temperature, and that they were probably not water-saturated.

5.5 Rheologic Critical Melt Percentage

The migmatites formed by partial melting, but did they migrate? Once there is enough melt to form an interconnected network, melt segregation should occur. This is called the permeability threshold, and can be less than 10% for felsic melts in migmatites (Sawyer, 1996). When there is sufficient melt to cause the entire framework to break down, the condition for melt mobility is met, and has been termed the rheologically critical melt percentage (RCMP) (Arzi, 1978). Estimates of the RCMP range from 10% to greater than 40%; this depends on the range of grain size and shapes, the mineralogy of the protolith, whether there is a shape-preferred orientation, and whether there is shearing during melting. The RCMP is significantly lowered by deformation, thereby enhancing melt segregation and (potential) mobility (Sawyer, 1996). Percentage of leucosome in the study area ranges from 10 to 35%. The region was also deformed, therefore the system was probably above the RCMP and some of the melt should have migrated. Field evidence suggests that leucosomes accumulated and migrated locally (Fig. 2.3), but there were no mappable plutons. The largest

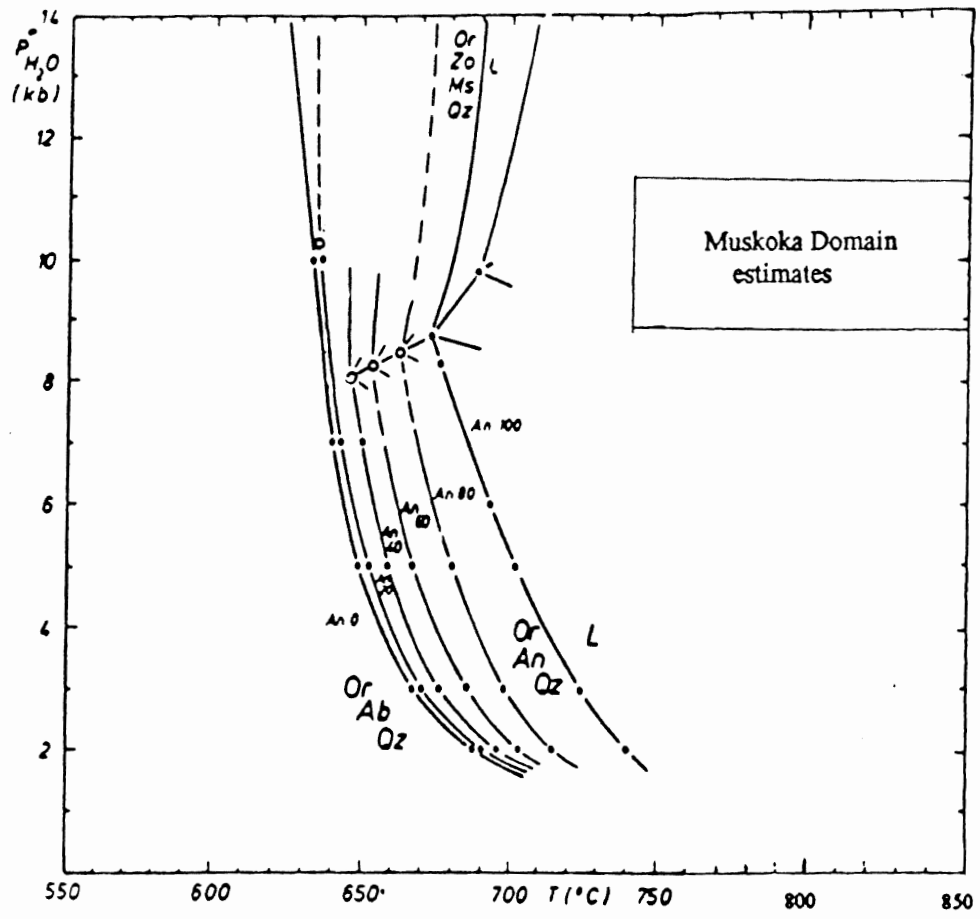

Figure 5.4. Solidus phase relations in the granite system Qz-Or-Ab-An-H_2O. Melting temperatures are higher for increased An content. If wet melting applies to the rocks of this study area, the pressure-temperature estimates puts them above the liquidus. Therefore the system would be totally molten. This suggests water-undersaturated conditions. Modified after Johannes, 1985.

accumulation of leucosome in the study area is 0.5m × 3.0m. Why did the melt stay in the system?

5.6 Melt Migration

For some reason(s) the melt was not extracted efficiently. There are three possibilities: (1) Was there some kind of barrier to melt migration? Regional tectonic interpretation suggest Muskoka Domain migmatites formed where CMB rocks were thrust over CGB along the CMBbtz (Culshaw et al., 1997; Timmermann et al., 1997). This raises the possibility that the structurally overlying Parry Sound Domain granulites or their equivalents may have formed an impermeable lid. (2) Did partial melting occur on a geologically rapid time scale, followed by quenching, thereby restricting the time for melt escape? This is the least favoured hypothesis because high-grade metamorphism occurred from 1079 -1064 Ma (Timmermann et al., 1997), a span of 15 My; this is not a short time period. Furthermore, petrology indicates that the rocks re-equilibrated. (3) Or did melt migration occur laterally between layers of the protolith? Volume changes (due to melting) and/or applied differential stress on a heterogeneous protolith may create mean normal stress differences, thereby driving convection and melt segregation laterally. Brown et al. (1995) proposed this mechanism to explain the widespread development of stromatic migmatites.

5.7. Summary

In situ anatexis is the most likely cause of formation of the Muskoka Domain migmatites. Is has been suggested that plagioclase should be more calcic, and alkali feldspar

should be more potassic in the leucosome of a migmatite complex formed by partial melting. This fractionation was observed in a few of the samples, however the difference is much smaller than expected. Even if equilibrium melting produced the leucosomes, some further re-equilibration would have been necessary to produce similar feldspar compositions between leucosome and mesosome or melanosome. Since the protolith was an orthogneiss of granodioritic composition, the compositions of the feldspars now are probably similar to what they were before migmatization.

Pressure and temperature estimates from other rocks in the area are well above the wet granite solidus. Therefore the system was probably not water-saturated.

The percentage of leucosome in the study area ranges from 10 to 35% of the outcrops. These amounts, coupled with the extent of deformation in the area, suggest the system was above the RCMP. However, there is only evidence for local melt migration. Why was the extraction method not efficient for the melt to leave the system? This question can only be answered with three more questions:

(1) Was there a barrier to upwards melt migration?

(2) Was melting a rather rapid process, followed by quenching?

(3) Was the melt driven laterally, due to pressure gradients between the layers of the migmatite?

CHAPTER 6 - CONCLUSIONS

6.0 Conclusions

The widespread distribution of highly migmatitic orthogneisses in the Muskoka Domain requires an explanation. These rocks lie in the immediate footwall of a crustal-scale imbricate zone, and their origin is therefore of regional significance. Migmatites are heterogeneous on an outcrop scale; stromatic migmatites may be proximal to large, diffuse cross-cutting leucosomes.

Samples from a small representative area of the Muskoka Domain were subdivided into 4 types based upon the proportion and shape of leucosome, and the presence of mafic porphyroblasts. A typical mineral assemblage of mesosome or melanosome is hb + bt + pl + kf + opq + qz. All leucosomes are enriched in potassium feldspar relative to mesosome or melanosome; Type 4 migmatites are also enriched in quartz. Deformation in outcrop is especially noticeable parallel to the lineation. This is also evident on a microscopic scale as mosaic texture in feldspars and quartz, myrmekite, cross-hatch twinned microcline, quartz ribbons, and finer-grained recrystallized matrix in leucosome.

Plagioclase feldspars have a narrow compositional range in the oligoclase field and show normal zoning (if present). Potassium feldspar compositions are slightly more variable, and perthite is abundant. Amphiboles, biotites and orthopyroxenes have narrow compositional ranges as well. In some samples, plagioclase is more calcic, potassium feldspar is more potassic, and biotite and hornblende are more magnesian in the mesosome. These data are consistent with anatexis as the origin of the migmatites. However, the small

compositional differences between minerals (especially feldspar) suggest equilibration of melt with host and limited migration.

REFERENCES

Anovitz, L.M. & Essene E.J. 1990. Thermobarometry and pressure - temperature paths in the Grenville Province of Ontario. J. Petrology, **31**: 197-241.

Arzi, A.A.1978. Critical phenomena in the rheology of partially melted rocks. Tectonophysics, **44**: 173-184.

Ashworth, J.R. 1985. "Introduction" *In:* Migmatites. *Edited by* J.R. Ashworth. Blackie, Glasglow: 1-35pp.

Blatt, H. & Tracy R.J. 1996. Petrology: igneous, sedimentary, and metamorphic, Second Edition. W. H. Freeman and Company, New York: 529p.

Bowen, N.L. 1913. The melting phenomena of the plagioclase feldspars. American Journal of Science, **35**: 577-599.

Brown, M., Averkin, Y.A., McLellan, E.L. & Sawyer, E.W. 1995. Melt segregation in migmatites. Journal of Geophysical Research, **100**: 15 655-15 679.

Culshaw, N., Davidson, A., & Nadeau, L. 1983. Structural subdivisions of the Grenville Province in the Parry Sound - Algonquin region, Ontario. *In* Current Reasearch, Part B, Geological Survey fo Canada, Paper 83-1B: 243-252.

Culshaw, N., Jamieson, R.A., Ketchum, J.W.F., Wodicka, N., Corrigan, D., & Reynolds, P.H. 1997. Transect across the northwestern Grenville orogen, Georgian Bay, Ontario: Polystage convergence and extension in the lower orogenic crust. Tectonics, **6**: 966-982.

Hutchison, C.S. 1974. Laboratory Handbook of Petrographic Techniques. John Wiley & Sons, 527p.

Johannes, W. 1985. "The significance of experimental studies for the formation of migmatites" *In:* Migmatites. *Edited by* J.R. Ashworth. Blackie, Glasglow: 36-85pp.

Misch, P. 1968. Plagioclase compositions and non-anatectic origin of migmatitic gneisses in Northern Casacade mountains of Washington State. Contributions to Mineralogy and Petrology, **54**:189-224.

Nyman, M.W., Pattison, D.R.M., & Ghent, E.D. 1995. Melt extraction during formation of K-feldspar and sillimanite migmatites, west of Revelstoke, British Columbia. Journal of Petrology, **36**:351-372.

Pitcher, W.S. & Berger, A.R. 1972. The geology of Donegal. London: Wiley, 435pp.

Sawyer, E.W. 1996. Melt segregation and magma flow in migmatites: implications for the generation of granitic magmas. Transactions of the Royal Society of Edinburgh, **87**: 85-94.

Timmermann, H., Parrish, R.R., Jamieson, R.A., & Culshaw, N.G. 1997. Time of metamorphism beneath the Central Metasedimentary Belt boundary thrust zone, Grenville orogen, Ontario: Accretion at 1080 Ma? Canadian Jouranl of Earth Sciences, **34**: 1023-1029.

Vernon, R.H. (1998) Quartz and feldspar microsctructures in metamorphic rocks. Canadian Mineralogist.

White, A.J.R. (1966) Genesis of migmatites from the Palmer region of South Australia. Chemical Gelogoy, **1**:165-200.

Yardley, B.W.D. (1978) Genesis of the Skagit Gneiss migmatites, Washington, and the distinction between possible mechanisms of migmatization. Geologiacl Society of Amererica Bulletin, **89**: 941-951.

Appendix A - Staining Procedures

Procedure for staining samples (Hutchison, 1974):

I) Etch sample with hydrofluoric acid (49%) 15-20 seconds
II) Rinse sample with water
III) Immerse sample in cobaltinitrate stain 30-40 seconds
IV) Rinse sample with water
V) Let sample air dry

Cobaltinitrate stain: 15 cc (glacial) acetic acid
25 cc demineralized H_2O
12.5 g cobaltous nitrate [$Co(NO_3)\bullet 6\ H_2O$] (99.5%)
20.0 g sodium nitrate [$NaNO_2$] (96%)

Etching releases Ca, Na, and K from the surface of the rock slab, allowing it to react with the stain. This turns plagioclase potassium feldspar bright yellow, and plagioclase chalky white.

Appendix B - Petrographic Descriptions and Point-Counting Results

Sample: 95-1 **Type:** 1

Mineralogy:

mineral	modal %	size (mm)	mineral	modal %	size (mm)
pl	25.0	≤ 0.6	hb	34.3	≤1.0
kf	18.3	≤ 0.6	bt	3.0	≤1.0
qz	3.0	≤ 0.6	px	11.0	≤ 0.5
ap	2.0	≤ 0.2	opq	3.0	≤ 0.6
calcite	0.3		muscovite	rare	

Texture: homogeneous; granoblastic; opx in textural equilibrium hb, locally rims it; felsic bdaries curved to embayed; bt generally subordinate in size to hb.

Alteration: can be extensive in hb and px, usually to calcite; minor in fdsprs; bt replacing hb.

Microprobe data: see appendix B

Sample: 97-9 **Type:** 1

Mineralogy: felsic **Mineralogy:** mafic

mineral	modal %	size (mm)	mineral	modal %	size (mm)
pl	30.3	≤ 1.3	pl	19.7	≤ 1.3
kf	33.3	≤ 1.3	kf	19.0	≤ 1.3
mi	2.3	≤ 1.3	mi	-	-
qz	24.3	≤ 1.3	qz	8.9	≤ 1.3
ap	0.3	≤ 0.3	ap	1.1	≤ 0.3
hb	-	-	hb	17.9	≤ 1.3
bt	7.3	≤ 0.8	bt	27.2	≤ 1.3
px	-	-	px	-	-
opq	1.6	≤ 0.8	opq	2.2	≤ 1.6
calcite	0.3		calcite	0.3	

Texture: common mosaic; inequi.; grain boundaries generally curved, minor embayed.

Texture: inequi.; bt ribbons; almost granoblastic; mosaic minor.

Alteration: common in fdsprs

Alteration: abundant in hb, and fdsrps to calcite.

Boundary: sharp, defined by bt concentration

Microprobe data: see appendix B

Sample: BV-16
Mineralogy: felsic body
kf, pl, qz, bt + opq, ap, cal
Texture: mosiac common; inequi.; similar to 97-9 felsic

Alteration: can be extensive in hb; minor in fdsprs
Microprobe data: none

Type: 2
Mineralogy: mafic body
pl, kf, hb, bt, qz + opq, ap, cal
Texture: weak foliation defined by bt; mosaic common; less mafic minerals than 97-9, greater disparity in grain size.
Alteration: can be extensive in hb; minor in fdsprs

Sample: 97-4B
Mineralogy: leucosome

mineral	modal %	size (mm)
pl	15.4	≤ 1.3
kf	43.2	≤ 1.3
mi	2.0	
perthite	20.6	
qz	18.5	≤ 1.1
ap	-	-
hb	-	-
bt	-	-
opq	-	-
alter	-	-

Texture: pods ≤ 1.0 cm thick, cross-cutting and parallel to foliation; mosaic abundant; myrmekite common; p'blasts of felsic min.s; boundaries curved to embayed.
Alteration: minor in fdsprs.

Microprobe data: see appendix B

Type: 2
Mineralogy: mesosome

mineral	modal %	size (mm)
pl	29.2	≤ 1.6
kf	23.9	≤ 1.6
mi	0.6	
perthite	2.6	
qz	8.9	≤ 1.6
ap	0.9	≤ 0.2
hb	31.5	≤ 1.3
bt	1.3	≤ 1.6
opq	0.6	
alter	-	-

Texture: mosaic common; ap common accessory min.
Other: based on 96 counts, therefore NOT as accurate a count as others.

Alteration: can be extensive in hb; minor in fdsprs.

Sample: BV-17
Mineralogy: leucosome

mineral	modal %	size (mm)
pl	20.2	≤ 1.6
kf	57.8	≤ 1.6
mi	1.6	
perthite	15.6	
qz	3.6	≤ 1.6
ap	-	
hb	0.3	
bt	0.3	
opq	-	
alter	0.3	

Texture: inequigranular; abundant myrmekite and mosaic; curved to embayed boundaries; elongate qz.

Alteration: common in fdsprs
Microprobe data: see appendix B

Type: 2
Mineralogy: mesosome

mineral	modal %	size (mm)
pl	25.6	≤ 1.6
kf	36.3	≤ 1.9
mi	1.6	
perthite	15.3	
qz	2.3	≤ 1.4
ap	0.3	
hb	13.6	≤ 1.6
bt	2.0	≤ 1.6
opq	1.0	
alter	1.6	

Texture: inequi.; mosaic abundant; myrmekite common; boundaries in felsic min.s curved to embayed, straight to curved in hb; ti locally rims opq.
Alteration: common in fdsprs and hb.

Sample: BV-5
Mineralogy: leucosome
kf, qz, pl + bt, zr, opq, musc.
Texture: mosaic abundant; alkali-fdsprs and qz p'blasts ≥ 4cm abundant; mi abundant; perthite common; myrmekite common.
Alteration: can be extensive in fdsrprs and hb
Microprobe data: none

Type: 2
Mineralogy: mesosome
bt, hb, pl, kf, qz, + opq, ap, zr
Texture: boundary defined by bt accumulation; pods of leuc within; much less mi than in leuc; mosaic common; elongate qz.
Alteration: common in fdsprs; hb to chlorite common.

Sample: BV-14
Mineralogy: leucosome
pl, kf, qz
Texture: mosaic abundant; myrmekite common; elongate qz (ribbon?); qz and fdspr p'blasts; embayed bdaries; all min.s ≤ 1.9 mm.
Alteration: minor in fdsprs
Microprobe data: none

Type: 2
Mineralogy: melanosome
pl, bt, hb, kf, qz, + opq, ap, zr
Texture: pl adundant and generally larger than in leuc; mosaic common; embayed bdaries; bt and hb avg size 1.0 mm

Alteration: moderate in hb and fdsprs

Sample: BV-32
Mineralogy: leucosome patches
kf, qz, pl + ap
Texture: mosaic common; myrmekite rare; major constituents are kf with subordinate qz; mi common; perthite minor-common; pl minor; size: all ≤ 1.6 mm, avg 1.0 mm

Alteration: minor in fdsprs
Microprobe data: none

Type: 2
Mineralogy: mesosome
pl, hb, bt, qz, kf, opq + zr, ap, ti
Texture: moderate foliation; bt and hb often segregated; hb abundant and generally larger than bt; mafic min.s =40%; pl more abundant than in leuc; mosaic common; embayed bdaries; mi rare; all ≤ 1.3 mm.; ti locally rims opq.
Alteration: minor in fdsprs

Sample: 95-2
Mineralogy: matrix

mineral	modal %	size (mm)
plagioclase	13.6	≤ 1.6
quartz	15.9	≤ 1.6
biotite	8.3	≤ 1.5
opaque	1.3	≤ 1.5
alteration	1.3	

Texture: medium foliation defined by bt; abundant mosaic texture in fdsprs and qz; generally embayed boundaries; inequi.

Leucosomes ≤ 2.9mm in width
Mineralogy: kf (50%), qz, pl + bt, ap
Alteration: minor in fdsprs

Type: 3

mineral	modal %	size (mm)
alkali-fdspr	42.1	≤ 1.6
microcline	12.2	
hornblende	3.6	≤ 2.4
apatite	1.3	
		≤ 2.9mm

Alteration: abundant hb; minor fdspr and bt; probably minor hematite staining along grain boundaries.

Texture: few p'blasts of qz and fdsprs ≤2.9mm; qz ribbons; mosaic and mi abundant; pl minor; myrmekite rare.
Note: modal % of melanosome NOT neccessarily representative due to small thickness of leucosomes

Microprobe data: see appendix B

Sample: 97-7 **Type:** 3

Mineralogy: leucosome

mineral	modal%	size (mm)
pl	19.6	≤ 2.6
kf	39.6	≤ 3.8
mi	6.5	
perthite	11.3	
qz	20.6	≤ 2.6
ap	0.3	≤ 0.2
hb	-	-
bt	1.0	≤ 0.5
opq	-	-
ti	-	-
alter	0.6	

Texture: kf, qz, pl p'blasts; perthitic microcline common; mosaic abundant; myrmekite minor; embayed bdries.
Alteration: minor
Microprobe data: see appendix C

Mineralogy: melanosome

mineral	modal %	size (mm)
pl	33.6	≤ 2.6
kf	19.0	
mi	-	
perthite	-	
qz	11.0	≤ 2.6
ap	3.0	≤ 0.2
hb	17.6	≤ 3.5
bt	13.0	≤ 1.6
opq	2.3	≤ 1.3
ti	rare	≤ 0.2
alter	0.3	

Texture: mosaic common; hb generally lager; foliation defined by bt; bdaries curved to embayed.
Alteration: minor in fdsprs, bt

Mineralogy: neosome

mineral	modal %	size (mm)
pl	22.6	≤ 1.9
kf	35.3	≤ 1.9
mi	0.3	
perthite	1.6	
qz	28.0	≤ 2.7
ap	-	-
hb	3.0	≤ 1.1
bt	1.6	≤ 3.5
opq	1.0	
ti	-	-
alter	-	-

Texture: mosaic abundant; myrmekite minor; felsic bdaries generally embayed.

Alteration: minor

Sample: 97-5 **Type:** 3

Mineralogy: leucosome
pl (≤2.6mm), kf, qz (≤4.2mm)+ cal, musc

Texture: p'blasts of fdsprs and qz; elongate qz; mosaic abundant; curved to embayed bdaries; more pl than any other leuc; mi minor
Alteration: extensive in fdsprs to calcite

Microprobe data: none

Mineralogy: melanosome
pl (50%), hb (≤2.9mm), bt(≤2.3mm), kf, qz, opq + ti, cal, zr, ap, musc
Texture: foliation; mosaic common; mi rare; ti locally rims opq; embayed bdaries

Alteration: extensive in fdsprs (to calcite) and hb

Sample: 97-6 **Type:** 3

Mineralogy: leucosome
kf (≤ 3.5mm), qz, pl + bt, ap

Texture: p'blasts of qz and fdsprs; common myrmekite and mosaic; embayed bdaries.
Alteration: common in fdsprs
Microprobe data: none

Mineralogy: melanosome
pl (≤2.2mm), kf, qz, bt (≤1.0mm) +opq, ap, zr
Texture: wavy foliation – difficlut to see in thin section; mosaic abundant; perthite rare (≤3.2mm); mi rare; myrmekite rare
Alteration: common in fdsprs

Sample: 95-3 **Type:** 4

Mineralogy: leucosome

mineral	modal %	size (mm)
pl	2.0	≤ 2.6
kf	16.6	≤ 30.0
mi	24.3	
perthite	34.0	
qz	21.0	≤ 6.4
ap	-	-
hb	-	-
bt	-	-
opq	-	-
titanite	-	-
calcite	1.6	≤ 1.0
musc	0.3	≤ 0.6

Texture: qz, perthitic mi, fdsrps p'blasts; qz ribbons; mosaic abundant; myrmekite rare; bdaries curved.

Alteration: abundant to calcite and musc.

Mineralogy: melanosome

mineral	modal%	size (mm)
pl	17.0	≤ 1.3
kf	21.3	≤ 1.5
mi	4.6	≤ 0.6
perthite	0.6	≤ 1.0
qz	20.0	≤ 1.6
ap	1.3	≤ 0.3
hb	29.0	≤ 2.6
bt	4.6	≤ 1.8
opq	0.6	≤ 0.8
titanite	0.3	≤ 0.3
calcite	-	-
zr	0.3	

Texture: foliation defined by bt and hb; mosaic abundant; curved to embayed bdaries

Alteration: rare to minor

Mineralogy: mesosome

mineral	modal %	size (mm)
pl	10.0	≤ 1.3
kf	40.6	≤ 1.3
mi	10.6	
perthite	2.0	
qz	26.0	≤ 2.2
ap	1.0	≤ 0.3
hb	3.0	≤ 2.6
bt	5.6	≤ 1.3
opq	0.3	≤ 1.0
titanite	-	-
calcite	0.6	

Texture: hb p'blasts; mosaic abundant; qz elongate parallel to foliation defined by bt.

Alteration: minor

Microprobe data: none

Note: modal % of leucosome is NOT necessarily representative, due to large size of p'blasts relative to size of thin section, and bt nor hb p'blasts were in the thin section.

Sample: 97-4A **Type:** 4

Mineralogy: leucosome

kf (≤3.2mm), pl, qz (≤4.8mm) + hb, bt, opq, musc

Texture: kf (esp. perthite), pl, qz, hb+bt p'blasts; qz ribbons; mosaic abundant; myrmekite common; mi and perthite commom;

Alteration: locally extensive in fdsprs to calcite, extensive in bt; minor hb.

Microprobe data: none

Mineralogy: melanosome

pl (≤3.2mm), hb(≤3.8mm), kf, qz, bt + opq, ti, zr, musc

Texture: not as coarse as 97-10; p'blasts of hb; mosaic minor; ti locally rims opq

Alteration: minor

Sample: 97-8
Mineralogy: leucosome

mineral	modal %	size (mm)
pl	31.0	≤ 1.9
kf	23.3	≤ 6.4
mi	11.6	
perthite	4.3	
qz	19.6	≤ 6.4
ap	0.3	
hb	5.0	≤ 2.6
bt	1.3	≤ 1.3
opq	2.3	≤ .8
alter	-	-

Texture: p'blasts of hb, qz, kf, bt abundant; qz ribbons; mosaic abundant; myrmekite common; embayed bdaries.

Type: 4
Mineralogy: mesosome

mineral	modal %	size (mm)
pl	18.3	this will be
kf	43.0	recounted
mi	7.3	% are not
perthite	3.0	represent-
qz	17.6	ative
ap	-	
hb	0.6	
bt	7.6	
opq	1.3	
alter	1.0	

Texture: mosaic abundant; p'blasts of fdspr, bt and hb abundant; ti locally rims opq; myrmekite common; embayed bdaries;

Other: bdary between leuc and meso defined by hb foliation

Alteration: hematite in fdsprs rare to common.

Alteration: hematite in fdsprs rare to common

Microprobe data: see appendix C

Sample: 97-10
Mineralogy: leucosome

mineral	modal %	size (mm)
pl	27.6	≤ 2.6
kf	6.6	≤ 8.0
mi	6.0	
perthite	6.6	
qz	34.6	≤ 8.0
ap	-	-
hb	11.0	≤ 3.5
bt	2.6	
opq	3.6	≤ 1.6
alter	1.0	

Texture: hb, qz, perthitic mi p'blasts; mosaic, myrmekite abundant; embayed bdaries.

Alteration: extensive in fdsprs, hb p'blasts.

Microprobe data: see appendix C

Type: 4
Mineralogy: melanosome

mineral	modal %	size (mm)
pl	28.6	≤ 2.6
kf	3.6	≤ 1.9
mi	1.4	
perthite	-	-
qz	8.8	≤ 1.9
ap	0.7	≤ 0.2
hb	40.4	≤ 3.5
bt	8.0	≤ 2.9
opq	5.8	≤ 16
alter	1.4	

Texture: foliation; mosaic minor; myrmekite rare; embayed bdaries.

Alteration: can be xtensive in hb; minor in fdsprs.

APPENDIX C - Microprobe Analytical and Data Techniques

Analytical Methods:

Analyses were carried out on a JEOL 733 electron microprobe at Dalhousie University. It was equipped with four wavelength spectrometers and an Oxford Link eXL energy dispersive system. The energy dispersive system was used for all elements. Resolution of the energy disppersive sector was 137ev at 5.9Kev. Each spectrum was aquired for 40 seconds with an accelerating voltage of 15 Kv and a beam current of 15nA. Probe spot size was approximately I micron. The raw data was corrected using Link's ZAF matrix correction program.

Instrument calibration was performed on cobalt metal.
Instrument precision on cobalt metal (n=10) was ± 0.5% at 1 standard deviation.
Accuracy for major elements was ± 1.5% to 2.0% relative. Geological standards were used as controls. Detection limits for most elements using the energy dispersive system range from approximately 0.1-0.3%.

All analyses, excluding opaque minerals, were processed using MINPET Version 2.0. All diagrams using the microprobe data were generated using this program.

Table C1. Plagioclase compositions used for all microprobe analyses. Formulae calculated on the basis of 32oxygens.

Sample	95-1	95-1	95-2	95-2	95-2	95-2	95-2	97-10	97-10	BV-17
Analysis	1.7	2.3	1.2Lam	1.4C	1.5C	3.3R	3.5C	2.6C	2.7R	3.2C
Location	mafic	mafic	leuc	leuc	leuc	matrix	matrix	leuc	leuc	matrix
Mineral	plg	plg	plg	plg	plg	plg	plg	plg	plg	plg
SiO2	57.26	57.67	62.33	61.88	62.47	62.23	62.13	62.77	62.5	62.39
Al2O3	27.38	27.3	23.4	23.54	23.75	23.58	23.5	24.15	24.35	23.43
FeO	0.1	0.05	0.16	0.07	0.06	0	0.13	0	0.19	0.12
CaO	9.12	9.16	4.71	4.88	4.9	4.91	4.95	5.36	5.64	4.95
Na2O	6.32	6.2	8.83	8.6	8.37	8.59	8.53	8.76	8.68	8.61
K2O	0.07	0.03	0.14	0.24	0.25	0.17	0.18	0.22	0.21	0.23
Total	100.3	100.41	99.63	99.24	99.91	99.51	99.43	101.33	101.72	99.79
Si	10.236	10.281	11.086	11.05	11.064	11.071	11.068	10.993	10.935	11.079
Al	5.764	5.732	4.901	4.95	4.954	4.94	4.93	4.981	5.017	4.9
Fe2	0.015	0.007	0.024	0.01	0.009	0	0.019	0	0.028	0.018
Ca	1.747	1.75	0.898	0.934	0.93	0.936	0.945	1.006	1.057	0.942
Na	2.191	2.143	3.045	2.978	2.874	2.963	2.947	2.975	2.945	2.965
K	0.016	0.007	0.032	0.055	0.056	0.039	0.041	0.049	0.047	0.052
Sum	19.979	19.92	19.998	19.985	19.916	19.953	19.953	20.022	20.053	19.972
Ab	55.4	54.9	76.6	75.1	74.5	75.2	74.9	73.8	72.7	74.9
An	44.2	44.9	22.6	23.5	24.1	23.8	24	25	26.1	23.8
Or	0.4	0.2	0.8	1.4	1.5	1	1	1.2	1.2	1.3

Sample	97-10	97-10	97-10	97-10	97-10	97-4B	97-7	97-7	97-7	97-7	BV-17
Analysis	3.10C	3.11R	4.2Lam	4.3R	4.4C	2.8C	1.4C	1.7R	2.2C	3.2	2.6R
Location	melan	melan	leuc	leuc	leuc	matrix	melan	melan	leuc	leuc	leuc
Mineral	plg	plg	plg	plg	plg	plg	plg	plg	plg	plg	plg
SiO2	63.73	64.39	64.79	62.24	62.68	62.76	62.67	62.51	62.63	62.44	62.42
Al2O3	23.96	24.15	23.17	23.74	23.95	23.71	24.1	24	23.88	23.78	23.26
FeO	0.24	0.19	0.11	0.08	0.11	0.23	0.05	0.13	0.05	0.1	0.33
CaO	5.37	5.16	3.31	5.24	5.27	5.04	5.31	5.39	4.82	5.22	4.99
Na2O	7.87	8.24	6.26	8.54	8.24	8.93	7.53	8.09	8.4	7.7	8.63
K2O	0.27	0.14	0.38	0.14	0.22	0.13	0.37	0.26	0.16	0.16	0.09
Total	101.51	102.34	98.11	100	100.48	100.92	100.08	100.39	100.12	99.4	99.73
Si	11.104	11.116	11.478	11.032	11.045	11.045	11.062	11.029	11.064	11.09	11.095
Al	4.916	4.91	4.834	4.955	4.97	4.914	5.01	4.987	4.968	4.974	4.869
Fe2	0.035	0.027	0.016	0.012	0.016	0.034	0.007	0.019	0.007	0.015	0.049
Ca	1.002	0.954	0.628	0.995	0.995	0.95	1.004	1.019	0.912	0.993	0.95
Na	2.659	2.758	2.15	2.935	2.816	3.047	2.577	2.768	2.877	2.652	2.974
K	0.06	0.031	0.086	0.032	0.049	0.029	0.083	0.059	0.036	0.036	0.02
Sum	19.791	19.814	19.216	19.966	19.894	20.035	19.756	19.884	19.904	19.76	19.96
Ab	71.5	73.7	75.1	74.1	73	75.7	70.3	72	75.2	72	75.4
An	26.9	25.5	21.9	25.1	25.8	23.6	27.4	26.5	23.8	27	24.1
Or	1.6	0.8	3	0.8	1.3	0.7	2.3	1.5	0.9	1	0.5

Sample	97-7	97-8	97-8	97-8	97-9	97-9	97-9	97-9	97-9	BV-17
Analysis	3.3Lam	1.2Lam	2.7C	2.8R	1.3C	1.4	2.3C	2.4C	3.1C	3.1C
Location	leuc	leuc	matrix	matrix	mafic	mafic	bdary	bdary	felsic	matrix
Mineral	plg	plg	plg	plg	plg	plg	plg	plg	plg	plg
SiO2	63.03	62.9	62.72	62.31	62.29	63.36	62.34	62.33	63.37	62.8
Al2O3	23.94	23.67	23.25	23.73	23.92	23.39	23.98	23.91	23.05	23.62
FeO	0.22	0	0	0.19	0.1	0.18	0.08	0	0.1	0.03
CaO	5.29	4.85	4.65	4.77	5.6	4.68	5.53	5.41	4.72	4.87
Na2O	8.02	8.6	8.95	9.12	8.13	8.79	8.25	8.22	8.85	8.61
K2O	0.12	0.2	0.21	0.17	0.1	0.08	0.13	0.14	0.43	0.17
Total	100.82	100.29	99.84	100.38	100.24	100.6	100.44	100.05	100.76	100.24
Si	11.065	11.099	11.127	11.02	11.015	11.142	11.009	11.031	11.156	11.095
Al	4.949	4.919	4.858	4.942	4.981	4.844	4.987	4.983	4.779	4.915
Fe2	0.032	0	0	0.028	0.015	0.026	0.012	0	0.015	0.004
Ca	0.995	0.917	0.884	0.904	1.061	0.882	1.046	1.026	0.89	0.922
Na	2.73	2.943	3.079	3.128	2.788	2.997	2.825	2.821	3.021	2.95
K	0.027	0.045	0.048	0.038	0.023	0.018	0.029	0.032	0.097	0.038
Sum	19.838	19.933	20.004	20.084	19.9	19.937	19.926	19.899	20.012	19.944
Ab	72.8	75.4	76.8	76.9	72	76.9	72.4	72.7	75.4	75.4
An	26.5	23.5	22	22.2	27.4	22.6	26.8	26.5	22.2	23.6
Or	0.7	1.2	1.2	0.9	0.6	0.5	0.7	0.8	2.4	1

Sample	97-9	BV-17	BV-17	BV-17	BV-17	BV-17	BV-17	BV-17	BV-17
Analysis	3.3C	1.1	1.2C	1.3R	1.5Lam	1.6C	2.2Lam	2.3C	2.4R
Location	felsic	leuc	leuc	leuc	leuc	leuc	leuc	leuc	leuc
Mineral	plg	plg	plg	plg	plg	plg	plg	plg	plg
SiO2	63.23	62.99	62.36	63.07	63.47	63.3	63.07	62.83	62.6
Al2O3	23.52	23.49	23.4	23.5	23.57	23.5	23.36	23.55	23.28
FeO	0.03	0.15	0.07	0.14	0.07	0	0.06	0.12	0.13
CaO	4.73	5.09	5.05	4.96	4.77	4.93	4.79	5.12	4.84
Na2O	8.36	8.02	8.54	8.53	8.77	8.62	8.73	8.6	8.58
K2O	0.42	0.21	0.23	0.24	0.19	0.23	0.18	0.24	0.15
Total	100.42	99.95	99.67	100.44	100.9	100.71	100.25	100.56	99.61
Si	11.138	11.136	11.085	11.117	11.129	11.121	11.133	11.076	11.122
Al	4.879	4.891	4.898	4.878	4.867	4.862	4.856	4.889	4.871
Fe2	0.004	0.022	0.01	0.021	0.01	0	0.009	0.018	0.019
Ca	0.893	0.964	0.962	0.937	0.896	0.928	0.906	0.967	0.921
Na	2.855	2.749	2.943	2.915	2.982	2.937	2.988	2.94	2.956
K	0.094	0.047	0.052	0.054	0.043	0.052	0.041	0.054	0.034
Sum	19.893	19.809	19.955	19.922	19.943	19.934	19.948	19.97	19.93
Ab	74.3	73.1	74.4	74.6	76.1	75	75.9	74.2	75.6
An	23.2	25.6	24.3	24	22.9	23.7	23	24.4	23.5
Or	2.4	1.3	1.3	1.4	1.1	1.3	1	1.4	0.9

Table C2. Potassium feldspar compositions used for all mircoprobe analyses. Formulae calculated on the basis of 32 oxygens.

Sample	95-2	95-2	95-2	95-2	97-10	97-10	97-4B	97-4B	97-4B
Analysis	1.1	1.3	3.1	3.6	2.4	4.1perth	1.1	1.1	1.2
Location	leuc	leuc	matrix	matrix	leuc	leuc	leuc	leuc	leuc
Mineral	ksp	ksp	ksp	ksp	ksp	ksp	ksp	ksp	ksp
SiO2	64.77	65.35	64.8	64.86	65.44	66.5	64.8	65.43	64.26
Al2O3	18.58	18.74	18.8	18.93	18.82	19.23	18.73	18.89	18.67
FeO	0.01	0.02	0.02	0.06	0.03	0.03	0.04	0.01	0
CaO	0	0	0.03	0	0	0.1	0	0	0
Na2O	1.08	1.49	0.94	1	1.14	2.09	1.29	1.27	1.06
K2O	15.09	14.21	15.24	15.07	14.89	12.09	14.76	13.44	14.68
Total	99.96	100.23	100.31	100.55	100.8	100.41	100.09	99.89	99.46
Si	11.959	11.982	11.935	11.918	11.966	12.021	11.942	12.005	11.932
Al	4.04	4.046	4.078	4.096	4.053	4.094	4.065	4.082	4.083
Fe2	0.002	.003	0.003	0.009	0.005	0.005	0.006	0.002	0
Ca	1.750	0	0.006	0	0	0.019	0	0	0
Na	0.387	.53	0.336	.356	0.404	0.733	0.461	0.452	0.382
K	3.55	3.324	3.581	3.533	3.474	2.788	3.47	3.146	3.478
Sum	20.014	19.945	20.01	20.011	19.973	19.713	20.016	19.809	20.002
Ab	9.8	13.8	8.6	9.2	10.4	20.7	11.7	12.6	9.9
An	0	0	0.2	0	0	0.5	0	0	0
Or	90.2	86.2	91.3	90.8	89.6	78.8	88.3	87.4	90.1

Sample	97-4B	97-7	97-7	97-7	97-7	97-7	97-7	97-7	97-8
Analysis	2.6	1.5	1.9	2.1	2.3	2.5	2.6	3.4perth	1.4inplg
Location	matrix	melan	melan	leuc	leuc	leuc	leuc	leuc	leuc
Mineral	ksp	ksp	ksp	ksp	ksp	ksp	ksp	ksp	ksp
SiO2	65.05	65.35	64.64	64.48	65.29	64.8	65.02	65.4	65.38
Al2O3	18.89	18.89	18.55	18.82	18.87	18.91	18.77	19.07	18.9
FeO	0.22	0	0.03	0.08	0.09	0	0	0.1	0.06
CaO	0	0	0	0.13	0.04	0.09	0.03	0.06	0
Na2O	1.54	0.91	0.7	1.12	1.15	1.52	1.53	1.24	1.54
K2O	13.84	14.58	15.07	14.68	14.16	14.22	13.94	14.47	14.17
Total	100.07	100.44	99.76	99.87	100.28	100.39	99.99	100.72	100.79
Si	11.948	11.974	11.977	11.919	11.974	11.916	11.964	11.942	11.946
Al	4.086	4.076	4.048	4.097	4.076	4.095	4.067	4.101	4.067
Fe2	0.034	0	0.005	0.012	0.014	0	0	0.015	0.009
Ca	0	0	0	0.026	0.008	0.018	0.006	0.012	0
Na	0.548	0.323	0.251	0.401	0.409	0.542	0.546	0.439	0.546
K	3.243	3.408	3.562	3.462	3.313	3.336	3.272	3.371	3.303
Sum	19.935	19.892	19.955	19.999	19.892	20.029	19.955	19.934	19.986
Ab	14.5	8.7	6.6	10.3	11	13.9	14.3	11.5	14.2
An	0	0	0	0.7	0.2	0.5	0.2	0.3	0
Or	85.5	91.3	93.4	89	88.8	85.6	85.6	88.2	85.8

Table C3. Biotite compositions for all microprobe analyses. Formulae calculated based on 22 oxygens.

Sample	95-1	95-1	95-2	95-2	97-10	97-10	97-10	97-4B	97-7	BV-17
Analysis	1.5	2.7	3.4	3.9	2.2	3.4	3.5	1.9	1.6	3.6
Location	matrix	matrix	matrix	matrix	leuc	matrix	matrix	leuc	melan	matrix
Mineral	bt	bt	bt	bt	bt	bt	bt	bt	bt	bt
SiO2	37.65	37.06	36.17	36.77	37.15	37.33	37.69	37.13	36.53	37.03
TiO2	2.92	3.88	4.31	4.36	4.05	3.64	3.71	4.01	4.43	3.97
Al2O3	14.9	14.64	14.24	14.26	14.64	13.83	14.01	13.68	13.75	14.17
FeO	14.75	15.59	19.05	18.94	18.34	18.3	18	18	18.94	16.28
MnO	0.04	0.02	0.3	0.29	0.19	0.14	0.27	0.22	0.52	0.25
MgO	15.11	14.28	10.92	11.32	11.53	12.05	12.6	12.53	11.09	12.69
BaO	0.11	0.9	0.09	0.23	0.17	0.22	0.1	0.23	0.43	0.41
Na2O	0.05	0.09	0.17	0.14	0.06	0.17	0.08	0.1	0.11	0.17
K2O	8.82	8.98	9.31	9.72	9.7	8.61	9.76	9.63	9.64	9.09
Total	94.35	95.44	94.56	96.03	95.83	94.29	96.22	95.53	95.44	94.06
Si	5.664	5.583	5.601	5.614	5.64	5.728	5.689	5.667	5.622	5.672
AlIV	2.336	2.417	2.399	2.386	2.36	2.272	2.311	2.333	2.378	2.328
AlVI	0.304	0.18	0.198	0.178	0.258	0.227	0.179	0.126	0.114	0.228
Ti	0.33	0.44	0.502	0.501	0.463	0.42	0.421	0.46	0.513	0.457
Fe2	1.856	1.964	2.467	2.418	2.329	2.348	2.272	2.297	2.438	2.085
Mn	0.005	0.003	0.039	0.038	0.024	0.018	0.035	0.028	0.068	0.032
Mg	3.389	3.207	2.521	2.577	2.61	2.756	2.835	2.851	2.544	2.898
Ba	0.006	0.053	0.005	0.014	0.01	0.013	0.006	0.014	0.026	0.025
Na	0.015	0.026	0.051	0.041	0.018	0.051	0.023	0.03	0.033	0.05
K	1.693	1.726	1.839	1.893	1.879	1.685	1.879	1.875	1.893	1.776
Sum	15.598	15.599	15.622	15.66	15.591	15.518	15.65	15.681	15.629	15.551
Mg_FeMg	0.65	0.62	0.51	0.52	0.53	0.54	0.56	0.55	0.51	0.58

Sample	97-8	97-8	97-9	97-9	97-9	97-9	BV-17	BV-17	BV-17	BV-17
Analysis	1.5	2.2	1.2	2.1	2.2	3.2	1.7	2.5	3.5	3.7
Location	leuc	matrix	mafic	mafic	mafic	felsic	leuc	leuc	matrix	matrix
Mineral	bt	bt	bt	bt	bt	bt	bt	bt	bt	bt
SiO2	36.45	37.04	36.86	37.16	36.97	35.88	36.19	36.77	36.55	37.12
TiO2	4.02	3.6	4.25	3.91	4.05	4.75	4.57	5.61	5.21	4.83
Al2O3	13.71	14.26	14.09	14.53	14.77	14.11	13.26	13.44	13.1	13.32
FeO	18.23	17.95	17.03	17.69	17.38	19.07	18.39	19.04	18.92	19.07
MnO	0.6	0.2	0.22	0.11	0	0.28	0.26	0.45	0.33	0.14
MgO	11.9	12.89	12.54	12.29	12.11	10.77	11.26	10.98	11.1	11.41
BaO	0.14	0.14	0.14	0.2	0.14	0.46	0.2	0.28	0.1	0.11
Na2O	0.2	0.06	0.11	0.05	0.03	0.32	0.14	0.17	0.11	0.14
K2O	9.56	9.46	9.53	9.62	9.62	9.79	9.15	9.48	9.5	9.48
Total	94.81	95.6	94.77	95.56	95.07	95.43	93.42	96.22	94.92	95.62
Si	5.634	5.641	5.634	5.641	5.627	5.548	5.657	5.603	5.639	5.671
AlIV	2.366	2.359	2.366	2.359	2.373	2.452	2.343	2.397	2.361	2.329
AlVI	0.13	0.198	0.17	0.239	0.275	0.117	0.098	0.015	0.019	0.068
Ti	0.467	0.412	0.489	0.446	0.464	0.552	0.537	0.643	0.605	0.555
Fe2	2.356	2.286	2.177	2.246	2.212	2.466	2.404	2.426	2.441	2.437
Mn	0.079	0.026	0.028	0.014	0	0.037	0.034	0.058	0.043	0.018
Mg	2.742	2.926	2.858	2.781	2.748	2.483	2.624	2.494	2.553	2.599
Ba	0.008	0.008	0.008	0.012	0.008	0.028	0.012	0.017	0.006	0.007
Na	0.06	0.018	0.033	0.015	0.009	0.096	0.042	0.05	0.033	0.041
K	1.885	1.838	1.858	1.863	1.868	1.931	1.825	1.843	1.87	1.848
Sum	15.727	15.712	15.621	15.616	15.584	15.71	15.576	15.546	15.57	15.573
Mg_FeMg	0.54	0.56	0.57	0.55	0.55	0.5	0.52	0.51	0.51	0.52

Table C4. Amphibole compositions for all microprobe analyses. Formulae calculated based on 23 oxygens. Fe^{+3} calculated assuming (B + C + T) = 15.00

Sample	95-1	95-1	95-1	95-1	95-1	97-10	97-10	97-10	97-10
Analysis	1.4	1.8	2.1	2.4	2.8	3.2	3.3	2.1	3.1
Location	mafic	mafic	mafic	mafic	mafic			leuc	melan
Mineral	hb	hb	hb	hb	hb	hb	hb	hb	hb
SiO2	42.29	42.64	43.1	42.67	42.73	42.85	43.14	42.47	43.38
TiO2	1.4	1.26	1.45	1.49	1.33	1.52	1.56	1.32	1.47
Al2O3	12.22	12.21	12.67	12.55	12.36	10.63	10.59	10.75	10.49
FeO	15.57	15.18	15.29	15.22	15.21	18.17	17.95	17.47	18.22
MnO	0.22	0.23	0.25	0.28	0.2	0.34	0.65	0.48	0.43
MgO	11.1	11.32	11.16	11.41	11.21	9.92	9.7	9.9	10.02
CaO	10.91	10.99	10.88	11.13	10.77	11.82	11.49	11.95	11.88
Na2O	1.51	1.69	1.71	1.74	1.78	1.76	1.62	1.45	1.72
K2O	0.92	0.9	0.94	0.88	0.95	1.5	1.73	1.45	1.5
Total	96.14	96.42	97.45	97.37	96.54	98.51	98.43	97.24	99.11
Si	6.34	6.373	6.376	6.318	6.383	6.441	6.495	6.441	6.477
AlC	1.66	1.627	1.624	1.682	1.617	1.559	1.505	1.559	1.523
AlC	0.497	0.522	0.584	0.506	0.558	0.323	0.372	0.361	0.322
Fe3	0.495	0.415	0.396	0.428	0.403	0.195	0.186	0.252	0.194
Ti	0.158	0.142	0.161	0.166	0.149	0.172	0.177	0.151	0.165
Mg	2.481	2.522	2.461	2.518	2.497	2.223	2.177	2.238	2.23
Fe2C	1.355	1.384	1.383	1.364	1.38	2.066	2.047	1.963	2.062
MnC	0.014	0.014	0.016	0.017	0.013	0.022	0.041	0.035	0.027
Fe2B	0.102	0.098	0.113	0.092	0.117	0.023	0.027	0	0.019
MnB	0.014	0.015	0.016	0.018	0.013	0.022	0.042	0.027	0.027
Ca	1.752	1.76	1.725	1.766	1.724	1.904	1.853	1.942	1.9
NaB	0.132	0.128	0.146	0.125	0.147	0.051	0.078	0.031	0.053
NaA	0.307	0.362	0.344	0.375	0.369	0.462	0.395	0.395	0.445
K	0.176	0.172	0.177	0.166	0.181	0.288	0.332	0.281	0.286
Sum	15.483	15.534	15.522	15.541	15.55	15.749	15.727	15.676	15.731

Sample	97-4B	97-4B	97-4B	97-7	97-8	97-8	97-9	BV-17	BV-17	BV-17
Analysis	1.5	2.5	2.7	1.1	2.3	2.4	1.1	1.8	3.8	3.9
Location	leuc	matrix	matrix	melan	matrix	matrix	mafic	leuc	matrix	matrix
Mineral	hb	hb	hb	hb	hb	hb	hb	hb	hb	hb
SiO2	42.33	42.12	42.34	42.15	42.32	42.16	42.41	41.81	41.94	42.11
TiO2	1.76	1.61	1.45	1.32	1.51	1.55	1.65	2.09	2.02	2.38
Al2O3	10.16	10.42	10.51	10.73	10.54	10.44	10.67	10.36	10.79	10.4
FeO	16.93	17.93	18.15	17.85	17.13	17.1	16.97	18.1	18.1	17.91
MnO	0.36	0.35	0.6	0.35	1.14	0.92	0.47	0.53	0.61	0.56
MgO	10.6	9.88	9.74	9.91	10.48	10.5	10.1	9.27	9.43	9.25
CaO	11.18	11.74	11.76	11.91	11.1	11.16	11.14	11	11.15	11.13
Na2O	1.9	1.8	1.93	1.63	1.71	1.74	1.74	1.82	1.65	1.78
K2O	1.44	1.43	1.47	1.49	1.42	1.39	1.32	1.58	1.56	1.56
Total	96.66	97.28	97.95	97.34	97.35	96.96	96.47	96.56	97.25	97.08
Si	6.448	6.414	6.42	6.402	6.386	6.39	6.463	6.438	6.39	6.451
AlC	1.552	1.586	1.58	1.598	1.614	1.61	1.537	1.562	1.61	1.549
AlC	0.27	0.283	0.296	0.322	0.259	0.253	0.378	0.317	0.326	0.327
Fe3	0.256	0.214	0.197	0.272	0.456	0.423	0.25	0.204	0.258	0.154
Ti	0.202	0.184	0.165	0.151	0.171	0.177	0.189	0.242	0.231	0.274
Mg	2.407	2.243	2.202	2.244	2.358	2.372	2.294	2.128	2.142	2.112
Fe2C	1.842	2.052	2.101	1.989	1.683	1.716	1.859	2.075	2.003	2.096
MnC	0.023	0.023	0.038	0.022	0.072	0.059	0.03	0.034	0.039	0.036
Fe2B	0.059	0.017	0.003	0.006	0.023	0.028	0.054	0.052	0.044	0.044
MnB	0.023	0.023	0.039	0.023	0.073	0.059	0.031	0.035	0.04	0.037
Ca	1.825	1.916	1.91	1.938	1.795	1.812	1.819	1.815	1.82	1.827
NaB	0.093	0.045	0.048	0.033	0.109	0.1	0.096	0.099	0.096	0.092
NaA	0.468	0.486	0.52	0.447	0.391	0.411	0.418	0.445	0.392	0.436
K	0.28	0.278	0.284	0.289	0.273	0.269	0.257	0.31	0.303	0.305
Sum	15.748	15.764	15.804	15.736	15.665	15.68	15.674	15.755	15.695	15.741

Table C5. Orthopyroxene compositions for all microprobe analyses. Formula calculated based on 6 oxygens.

Sample	95-1	95-1	95-1	95-1
Analysis	1.6	2.2	2.5	2.6
Location	mafic	mafic	mafic	mafic
Mineral	opx	opx	opx	opx
SiO2	51.52	51.29	51.97	51.5
Al2O3	1.95	1.72	1.76	1.71
FeO	25.01	25.55	25.54	25.35
MnO	0.83	0.79	0.64	0.76
MgO	19.85	19.51	19.72	19.79
CaO	0.3	0.3	0.3	0.28
Total	99.49	99.24	99.93	99.39
Si	1.956	1.957	1.967	1.959
AlIV	0.044	0.043	0.033	0.041
AlVI	0.043	0.035	0.046	0.036
Mg	1.123	1.11	1.113	1.122
Fe2	0.793	0.807	0.809	0.801
Mn	0.027	0.026	0.021	0.024
Ca	0.012	0.012	0.012	0.011
Sum	4	4	4	4

Table C6. Opaque minerals analyses.

Sample	95-2-3	95-2-3	97-81	97-8-2	97-8-2	97-4B-1	97-4B-1	21
Point	21	22	29	35	36	46	47	43.00
SiO2	0.24	1.51	0.18	0.30	0.22	0.22	0.22	3.04
TiO2	8.25	57.25	0.19	46.90	16.30	12.48	45.11	55.96
FeO	77.25	24.67	87.64	46.36	72.13	75.32	49.29	29.78
Total	85.74	83.43	88.00	93.56	88.64	88.02	94.63	88.78

Sample	97-7	97-7	97-10	97-10	97-10	97-10	97-10	97-10
Point	9.00	10.00	11.00	12.00	13.00	26.00	27.00	28.00
SiO2	0.08	0.29	0.19	0.18	1.19	0.16	0.22	0.16
TiO2	9.31	48.09	12.21	9.04	56.50	0.44	47.30	25.72
FeO	79.56	47.80	77.71	80.07	28.89	90.01	49.28	67.85
Total	88.94	96.17	90.12	89.30	86.58	90.61	96.80	93.74